Archaeal Membranes: in silico modelling and design

by

Miguel Amaral

December, 2024

A thesis submitted to the
Graduate School
of the
Institute of Science and Technology Austria
in partial fulfillment of the requirements
for the degree of
Doctor of Philosophy

Committee in charge:

Jérémie Palacci, Chair
Anđela Šarić
Edouard Hannezo
Oded Farago

The thesis of Miguel Amaral, titled *Archaeal Membranes: in silico modelling and design*, is approved by:

Supervisor: Anđela Šarić, ISTA, Klosterneuburg, Austria

Signature: _____

Committee Member: Edouard Hannezo, ISTA, Klosterneuburg, Austria

Signature: _____

Committee Member: Oded Farago, Ben Gurion University, Be'er Sheva, Israel

Signature: _____

Defense Chair: Jérémie Palacci, ISTA, Klosterneuburg, Austria

Signature: _____

Signed page is on file

ISTA Thesis, ISSN: 2663-337X

ISBN: 978-3-99078-046-6

I hereby declare that this thesis is my own work and that it does not contain other people's work without this being so stated; this thesis does not contain my previous work without this being stated, and the bibliography contains all the literature that I used in writing the dissertation.

I accept full responsibility for the content and factual accuracy of this work, including the data and their analysis and presentation, and the text and citation of other work.

I declare that this is a true copy of my thesis, including any final revisions, as approved by my thesis committee, and that this thesis has not been submitted for a higher degree to any other university or institution.

I certify that any republication of materials presented in this thesis has been approved by the relevant publishers and co-authors.

Signature: _____

Miguel Amaral
December, 2024

Signed page is on file

Abstract

Across the tree of life, distinct designs of cellular membranes have evolved that are both stable and flexible. In bacteria and eukaryotes this trade-off is accomplished by single-headed lipids that self-assemble into flexible bilayer membranes. By contrast, archaea in many cases possess both bilayer and double-headed, monolayer spanning bolalipids. This composition is believed to enable extremophile archaea to survive harsh environments. Here, through the creation of a minimal computational model for bolalipid membranes, we discover trade-offs when forming membranes using lipids of a single type. Similar to living archaea, we can tune the stiffness of bolalipid molecules. We find that membranes made out of flexible bolalipid molecules resemble bilayer membranes as they can adopt U-shaped conformations to enable higher curvatures. Conversely, rigid bolalipid molecules, like those found in archaea at higher temperatures, preferentially take on a straight conformation to self-assemble into liquid membranes that are stable, stiff, prone to pore formation, and which tear during membrane reshaping. Strikingly, however, our analysis reveals that it is possible to achieve the best of both worlds – membranes that are fluid, stable at high temperatures and flexible enough to be reshaped without leaking – through the inclusion of a small fraction of bilayer lipids into a bolalipid membrane. Additionally, the curvature-dependent softening of bolalipid membranes made of lipids with tension-sensitive conformation can also enable high rigidity at low curvatures while softening at high curvatures, making the membrane effectively a plastic material. Taken together, our study compares the different membrane designs across the tree of life and indicates how combining lipids can be used to resolve trade-offs when generating membranes for (bio)technological applications.

About the Author

Miguel Amaral completed a MSc in Physics in 2017 and a MSc in Computer Science in 2019, both at the University of Porto, before joining Anđela Šarić's research group in 2020 at University College London for his PhD. In January 2022, the research group moved to ISTA. His main interests include modelling and characterizing at the micro and meso-scale membrane reshaping, and solving computational challenges that often pop up in coarse-grain modelling. He started the group's work on modelling archaeal membranes and together with collaborators has published the findings.

List of Collaborators and Publications

Most of the original content of this thesis (Chapters 1 to 3 and Section 4.1) appears in the following preprint:

Miguel Amaral et al. *Stability vs Flexibility: Reshaping Monolayer and Bilayer Archaeal Membranes in Silico*. Oct. 2024. DOI: 10.1101/2024.10.18.619072

Paper author contributions: MA performed computer simulations and analysis and wrote the manuscript. FF performed patch closing simulations, contributed to computer simulations and modelling of fluctuation spectrums, and wrote the manuscript. XJ contributed to initial budding simulations and the manuscript. BB co-supervised the project and edited the manuscript. AŠ conceived the study, supervised the project and edited the manuscript.

Table of Contents

List of Figures

List of Tables

List of Movies

Available in [3, SI]

1 Self-assembly of flexible bolalipid molecules into a flat membrane ($k_{\mathrm{bola}} = 0$).

2 Close-up view of a flat membrane, with tail beads shown like sticks.

- 2.a Membrane made of bilayer-forming molecules at $T_{\mathrm{eff}} = 1.1$ (same bilayer membrane as in tethers of Fig. 4.1C)
- 2.b Membrane made of flexible bolalipid molecules ($k_{\mathrm{bola}} = 0$).
- 2.c Membrane made of rigid bolalipid molecules ($k_{\mathrm{bola}} = 5\, k_{\mathrm{B}}\, T$).

3 Fluctuating flat membrane patch of bolalipid molecules at $k_{\mathrm{bola}} = 0$ used for height fluctuation spectrum measurements.

4 Cylindrical membranes after equilibration, made of bolalipid molecules of intermediate stiffness ($k_{\mathrm{bola}} = 1\, k_{\mathrm{B}}\, T$) at the largest simulated radius $R \approx 17\sigma$.

5 Successful budding, showing only a cargo-centred cross-section.

- 5.a Budding from a membrane made of flexible bolalipid molecules ($k_{\mathrm{bola}} = 0$).
- 5.b Budding from a membrane made of bolalipid molecules of intermediate stiffness ($k_{\mathrm{bola}} = 1\, k_{\mathrm{B}}\, T$).
- 5.c Budding from a membrane made of completely stiff bolalipid molecules ($k_{\mathrm{bola}} = 5\, k_{\mathrm{B}}\, T$).
- 5.d Budding from a membrane made of a mixture of bolalipid and bilayer-forming lipid molecules, at bilayer fraction $f^{\mathrm{bi}} = 0.3$.

6 Rotating snapshot of a bud formed from a membrane made out of stiff rigid bolalipid molecules ($k_{\mathrm{bola}} = 5\, k_{\mathrm{B}}\, T$), showing several pores ($\epsilon_{\mathrm{mc}} = 3.25\, k_{\mathrm{B}}\, T$).

CHAPTER 1

Introduction

Every biological cell possesses a membrane that both separates its interior from its extracellular environment and confers the cell its shape. This membrane, while only a few nanometres thick, must be sturdy and impermeable to the leakage of small charged molecules like ions to allow the generation of an electrochemical gradient [42], but also flexible enough to be remodelled during essential cellular processes like cell division and vesicle formation [39]. These opposing goals, sturdiness and flexibility, lead to interesting and complex barrier designs across the tree of life.

At the cellular level, the tree of life is conventionally divided into three domains: the prokaryotes Bacteria and Archaea and the more complex Eukarya, which is thought to have evolved from a merger between Bacteria and Archaea [9], with the Asgard archaeal family identified as the closest genetic relatives to eukaryotes [54].

Archaea initially included organisms observed thriving in extreme environments like deep sea hydrothermal vents and acidic lakes, with record temperature being $120\,^{\circ}\mathrm{C}$, and pH at the sulphuric acid levels of $0.7\,\mathrm{pH}$ [60]. Archaean mesophiles were later found everywhere, from deep ocean sediments to animal guts [4, 58]. This shows the domain is able to withstand a wide range of temperature, pressure and acidity. This adaptability is hypothesized to be due to the dynamic and extreme primordial environment they evolved in. It may be that the original extreme conditions were essential to development of the complex features, that Eukarya then inherited. Orthogonally to the evolutionary question, Archaea's adaptability and endurance is alluring to biotechnology, and there is emergent research in applications in the food, chemical and pharmacology industries [55].

Archaea's resilience and adaptability has strong connections to the particularities of their cell membranes. Most Bacteria and Eukarya membranes are composed of self-assembled bilayer lipids, each an amphiphile composed of hydrophilic head group linked to two $\approx 4\,\mathrm{nm}$ long hydrophobic tails. These membranes are composed of two leaflets, each an arrangement of lipids stacked in a sheet with heads groups pointing outwards to the solvent and tails inwards towards the opposing leaflet. Lipids can diffuse within the membrane, making it a two-dimensional fluid surface. By contrast to diester bilayer lipids, many archaeal membranes contain molecules where two hydrophilic head groups are linked by a double hydrophobic chain that can span the membrane from side to side, called bolalipids, by similarity with the geometrically similar ancient weapon "bola" [26, 1]. By having ether linkages, bolalipids are also known as tetraethers, and archaeal bilayer lipids as diethers (see Fig. 1.1A for examples).

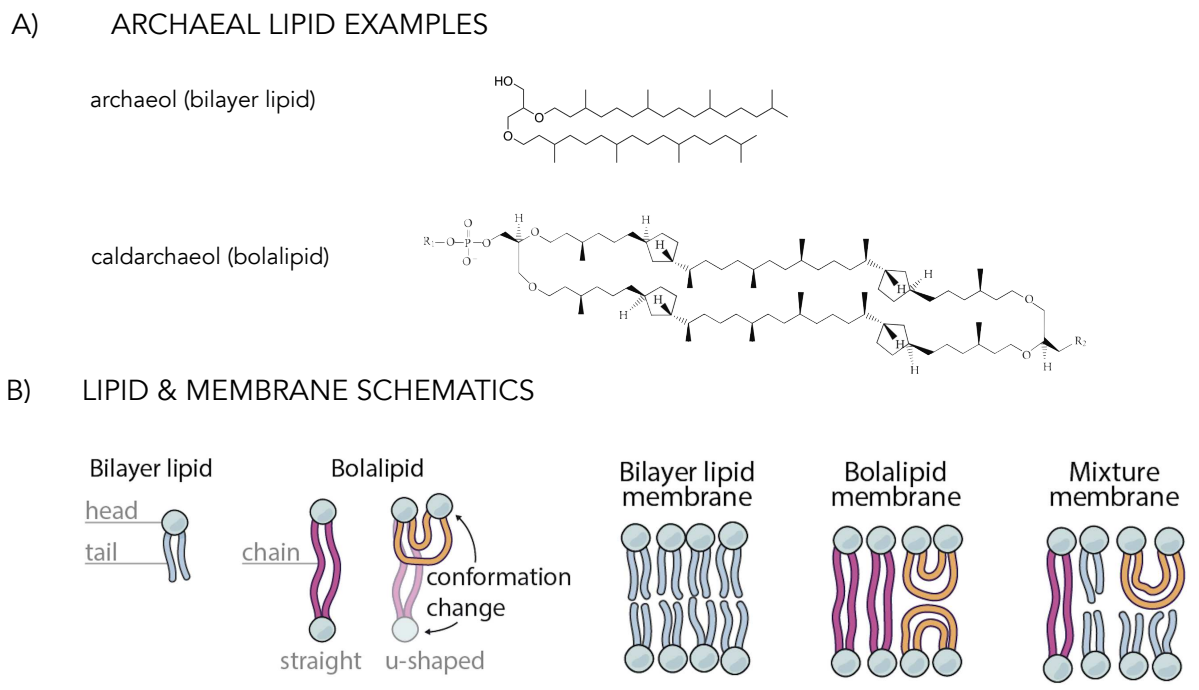

Figure 1.1: **Archaeal lipid chemistry and in-membrane conformation.**
(A) Structure of the diether bilayer lipid archaeol (left) and the tetraether bolalipid caldarchaeol including four cyclopentane rings (right), both present in the membrane of *Sulfolobus acidocaldarius*, a common archaeal model system that lives at high temperatures and low pH [46]. (B) (left to right) Schematics for a bilayer lipid, a bolalipid and its two in-membrane conformations, membranes made of bilayer molecules only, bolalipid molecules only, and a mixture of the two.

This different topology allows two distinct conformations in a membrane: either with one head in each side of the membrane, effectively the same as linking two antiparallel bilayer lipids, or with both heads on the same side of the membrane, forming what we will call an U-shape (Fig. 1.1B left). As an ensemble, bilayer and bolalipids can self-assemble into fluid lipid membranes of different architectures - as bilayer lipid membranes, bolalipid membranes or mixture membranes (Fig. 1.1B right). Thus far, in archaea the fraction of membrane lipids that are bolalipids varies with species from 2% to 90% [60, SI]. While these bolalipids have been found in mesophile organisms, sometimes as the main membrane component [50], for those extremophiles that do synthesize bolalipids, they are essential for survival in extreme environments [36].

In general, in response to the environment, cells adjust the lipid chemistry and the composition of their membranes to maintain a stable membrane fluidity, a process called homeoviscous adaptation. In archaea, this adaptation seems to happen mostly during the growth of the cell [45, 34]. The mixture of archaeal bilayer lipids with bolalipids does not necessarily phase separate: a lipid mixture of bolalipid extract with diester bilayer lipids self-assembled into vesicles where bolalipids were reported to pack tighter and have lower mobility than the bilayer lipids, without phase separating [62]. It is perhaps not surprising that higher growth temperature correlates with higher amount of bolalipids [34]: from physical point of view, a bolalipid is formed by constraining the degrees of freedom of two bilayer lipids by joining their tails. This extra constraint should increase order and thus temperature tolerance. For instance,

the cell membrane of one of the standard archaeal model systems, *Sulfolobus acidocaldarius*, which lives at $80\,^{\circ}\mathrm{C}$, can contain over 90% of bolalipids [41].

Archaeal lipids also exhibit dense packing, high viscosity, and low porosity to small molecules like protons [53], enabling the *Sulfolobus* membrane to sustain pH of 2 to 4 [25]. However, the ordering effect of bolalipids is not entirely desirable and thus possibly leads to a second difference w.r.t. Bacteria (and so Eukarya). While the later lipid hydrophobic tails' are (un)saturated fatty acids, in archaea, the lipids are isoprenoids, i.e. the hydrophobic tails possess branches along their lengths. This branching has been experimentally confirmed to increase permeability, specifically for archaeal bilayer lipids [35]. This agrees with molecular dynamics simulations, that show that branching is essential to maintain a liquid crystalline phase, either for bilayer lipids at low temperatures, or for bolalipids, by impeding the close packing of lipid tails and thus counteracting ordering [16]. These tail branches in archaeal lipids can be closed to form cyclopentane groups along archaeal lipid tails, up to 4 in bolalipids (e.g. the caldarchaeol in Fig. 1.1A) [53]. From their chemical structure it seems safe to assume that these rings enhance molecular rigidity and thus increase order. Supporting this, the number of these rings also increases with growth temperature [47]. Thus, both molecular rigidity and the bolalipid membrane fraction are tunable membrane properties that contribute to archaeal adaptability. Both of these factors in turn likely condition the amount of U-shaped conformers present in the membrane, which has been theorized to affect membrane mechanical properties [24, 64], thus providing a different path towards homeoviscous adaptation. We will also briefly comment that the membrane is not the only component responsible for the structural integrity of the cell. Covering their membrane, bacteria possess either a thick cell wall or an outer membrane, while Archaea have the S-layer, a network of paracrystalline membrane-anchored proteins 10's of nm tall that forms a protective casing over the membrane [41]. The repeating unit length for the S-layer has been reported for several species, varying from 10 to $40\,\mathrm{nm}$ [1]. Assuming the S-layer is quite rigid, this lattice size could set the characteristic length scale over which the archaeal membrane must maintain its integrity to be functional.

The exotic properties of archaeal membranes are also the source of great difficulties for researchers. Growing the organisms, extracting bolalipids or even synthesizing close enough analogues is difficult and only recently partially achieved [61]. Therefore, most of what we know about archaeal tetraether lipid membranes thus far has been collected from studying *in vitro* reconstituted membranes. For instance, the conformation of individual lipids in bolalipid membranes was first hinted at by crystallography [26], then studied at the water-air interface [5] or using NMR experiments on lipid vesicles [11]. This suggested the existence of U-shaped lipid conformations in archaeal type membranes (Fig. 1.1B). X-ray studies further localized the head-groups to only one side of the layer, further supporting the existence of lipids within the membrane with a U-shaped conformation [33]. Moreover, *in vitro* reconstituted vesicles primarily composed of bolalipids ($> 99\%$) can fuse with influenza virus particles at similar kinetic rates compared to bilayer vesicles, further suggesting that bolalipids exist in U-shape allowing for membrane remodelling and fusion [10]. Membrane properties like bending rigidity [62] or lipid phase [13] have also been measured in vesicles prepared from archaeal tetraether lipids to demonstrate that archaeal lipid derived membranes are unique in being stable up to temperatures of 80°C [13]. Furthermore, experiments with lipid vesicles made from synthetic bilayer lipids that include cyclopentane rings, which naturally appear in lipids of extremophilic archaea, showed that increasing the number of these rings increases membrane rigidity [8].

From the view point of membrane physics, the remodelling of bilayer membranes has been studied for decades using continuum models and computer simulations [52, 40, 23]. By contrast,

apart from the aforementioned experimental studies and a few studies either using fine-grained MD simulations or theory [12, 32, 24], little research has been devoted to investigating the properties of archaeal bolalipid membranes despite the obvious importance of this question from evolutionary, biophysics, and biotechnological perspectives. Particularly, membrane reshaping at the mesoscale has been largely neglected, although different membrane physics are expected to manifest.

Thus, the goal of this thesis is to offer the first exhaustive comparison of bolalipid membranes versus bilayer membranes, studying the role of bolalipids in archaeal membrane stability and mechanical properties, both of which govern membrane reshaping phenomena like vesicle trafficking and cytokinesis. We will do this by designing a novel coarse-grained minimal model for mixture membranes of bolalipids and bilayer lipids, and simulating mesoscale membrane remodelling phenomena, answering the question of what exactly happens in a membrane when bilayer lipids are linked together. We detail this approach in the next section.

1.1 Scope & Methodology

We propose to fill the gap in archaeal membrane modelling by designing the simplest coarsest model for extremophile archaeal membranes, involving mixtures of bilayer lipids and bolalipids. Our approach will be to bond together tail to tail two bilayer lipids from the Cooke model for bilayer lipid membranes [17]. We will describe this in detail later in Section 2.1, and for the rest of this chapter we will cover what is known regarding the Cooke model.

In the Cooke model, the solvent is implicit; the interactions with water are replaced by a short-range attractive interaction between hydrophobic components .Each lipid is represented by a 3 particles linked by fixed bond potentials and kept straight by angle potentials, i.e. well potentials dependent on the distance and angle formed by respectively 2 and 3 consecutive particles. With this model, the trade-off in accuracy results in much better performance, which is used to increase the duration of trajectories so that what will call meso-scale phenomena like lipid diffusion, membrane shape fluctuations and membrane reshaping can be observed. For instance, the Cooke model can simulate a 10nm radius vesicle budding from a membrane (roughly 5000 lipids, or to compare with the previous atomistic lattice size, a 70 by 70 lipid lattice) in a few days with current hardware. These timescales are based on using lipid diffusion to match simulation time units to real time units, which, as noted in the model's seminal paper, result in flip-flop rates (i.e. movement of lipids between membrane leaflets) that are orders of magnitude above those of lipid in real membranes. Since in this work we will not study dynamics, this fast flip-flopping is actually a time saver allowing us to quickly sample the equilibrium ensemble.

We will characterize the membrane by going over membrane theory, collecting relevant parameters that describe it, and then extract these parameters from simulations. We will also attempt to cover regimes where theory is not likely to provide an accurate description and thus where coarse-grained simulation makes a unique contribution. In the following two subsections we cover existing work related to these two tasks.

1.1.1 Membrane theory

While the lipid membrane is in a way a 2D fluid since lipids can flow in the transverse direction, it has structure. Bilayer membranes are composed of two leaflets, in which lipids must align

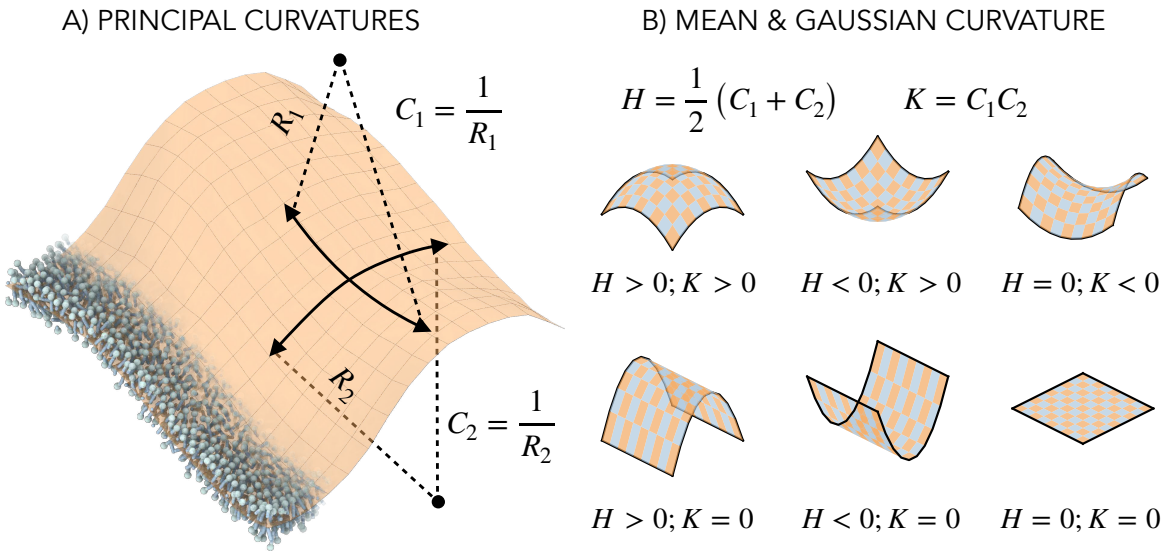

Figure 1.2: **Surface curvature schematics.** (A) A membrane can be described by is midsurface (orange), and at each point of this surface we can measure its principal curvatures (black arcs). The Helfrich Hamiltonian expresses the membrane bending energy in terms of mean and gaussian curvature, for which all possible combinations of signs are rendered in (B).

their tails roughly so they point outwards with their headgroups. Unlike a fluid, this structure resists deformations like stretching and bending.

The Helfrich hamiltonian. This bending cost can be expressed in first order in terms of the local principal curvatures C_1, C_2 of the membrane. Because it is just a first order expansion, it has no particular conditions on the specific structure of the membrane. When expressed in terms of the mean curvature $H = (C_1 + C_2)/2$ and the gaussian curvature $K = C_1 C_2$, this bending cost per membrane area is known as the Helfrich hamiltonian. The membrane energy is then an integration, over the area of the membrane S:

$$E_{\mathrm{B}} := \int_S \left(2\kappa \left(H - H_0\right)^2 + \bar{\kappa} K\right) dA \tag{1.1}$$

In this equation, κ its bending modulus and $\bar{\kappa}$ the gaussian curvature modulus. H_0 the spontaneous mean curvature, which accounts for a ground state preferred curvature.

Gaussian bending modulus. Due to the Gauss-Bonet theorem, the Gaussian term integrates to a constant for fixed topology and boundary. For a closed surface, this constant is $\bar{\kappa} 2\pi\chi(S)$, where $\chi(S)$ is the Euler characteristic of the surface. $\chi(S)$ is $2 - 2g$ where g is the genus of the surface, i.e. the number of handles one must attach to sphere to make a topologically equivalent surface to S. For instance, a sphere will have $g = 0$, while a torus will have genus $g = 1$; we note the torus is equivalent to a flat membrane in periodic boundary conditions. Continuum theory predicts bounds for ratio of the bending and gaussian moduli $\kappa/\bar{\kappa} \in [-2, -0.5]$, with agreement from measurements in experiments and simulations [31]. However, if one introduces dynamics, the evolution of the membrane is no longer a direct minimization of the Helfrich Hamiltonian and one must keep the local gaussian term. This can happen if, for instance, one models the hydrodynamic effects of the solvent [48].

Membrane tension. Tension is by definition the energy cost per area. Approximating near a rest membrane area A_0, we get:

$$E_{\mathrm{T}} := M\frac{(A-A_0)^2}{2A_0} \tag{1.2}$$

where M is the harmonic extensibility modulus. Tension is then:

$$\Sigma = \frac{dE_{\mathrm{T}}}{dA} = M\left(\frac{A}{A_0}-1\right)$$

In general, the membrane tension Σ is assumed to be isotropic in the membrane plane due to membrane fluidity. To obtain it from a simulation, consider the infinitesimal vertical compression of a horizontal square patch of membrane. Assuming volume conservation, it must expand horizontally equally in the x and y axis. This leads to the strains $\delta x/l_x =: \epsilon_x = \epsilon_y = -\frac{1}{2}\epsilon_z$. Writing down the corresponding potential energy change:

$$\begin{aligned}\delta U &= -\left(P_z l_x l_y \delta z + P_y l_x l_z \delta x + P_x l_y l_z \delta x\right)\\ &= -(P_z - \frac{P_x+P_y}{2})\frac{V}{l_z}\delta z\\ &= (P_z - \frac{P_x+P_y}{2}) l_z \delta A\end{aligned} \tag{1.3}$$

where δA is the change of horizontal area. Therefore $\Sigma = (P_z - \frac{P_x+P_y}{2})l_z$. While the volume conservation assumption is often assumed without justification in experimental papers, there is strong simulation support for the assumption of volume conservation from analysis of Martini membrane models for bilayer membranes [57]. In simulations of flat membrane patches in the xy plane with implicit solvent, we do not have this concern: the system does not cross the z plane thus $P_z = 0$.

Line tension. If the membrane possesses open edges, one adds the following term to the energy:

$$E_{\mathrm{P}} := \int_P \gamma dl \tag{1.4}$$

where P is then the membrane perimeter and γ the membrane edge tension, i.e. the energetic cost per length of open edge.

Lipid tilt. The Helfrich hamiltonian is expected to fit poorly the membrane behaviour at either qualitative deviations from the continuum theory base assumptions, or at sufficiently strong deformations. When lipid tails are rigid and not easily disordered, they can align with those of their neighbours, and become tilted relative to the membrane surface. This collective local ordering becomes a new degree of freedom that enters the hamiltonian [38]; such coordinated tilting can diminish the inner membrane volume, much like how flattening a parallelogram reduces its volume. This possibly works because lipids have large hydrophilic heads compared to their thinner tails, so that this flattening does not incur compression of neighbouring tails.

Membrane leaflets asymmetry. One can further detail the theory by separating the membrane into its two leaflets. Consider a membrane with thickness h where its leaflets have approximately equal and constant thickness $h/2$. Now bend it so it acquires mean curvature

H; its midplane, the surface at equal distance of the membrane exterior faces, keeps constant area A_{m}. However, each leaflet will respectively have an outside area difference w.r.t the membrane midplane $\Delta A_{\pm} = (1 \pm hH)\, A_{\mathrm{m}}$, in first order w.r.t. h, H. Assuming a leaflet cannot change its number of lipids, this will have in first order a cost $\kappa_A \left(\Delta A_{\pm}/\Delta A^0_{\pm} - 1\right)^2$, where $\Delta A^0_{\pm}$ is some rest equilibrium area difference. One can also add again a leaflet bending / gaussian modulus $\kappa_{\pm}, \bar{\kappa}_{\pm}$, where the leaflet is assumed to have been curved while holding its midplane, not the membrane's, at constant area. Taken together, these two contributions result, in first order, in the same terms present in the Helfrich (Eq. (1.1)), with different κ and C_0, both dependent on the membrane thickness h and the leaflet material properties and lipid area densities $\rho_{\pm} := n_{\pm}/A_{\mathrm{m}}$ [30], where $n_{\pm}$ are the respective leaflets number of lipids. Consequently, if one allows free flow of lipids between leaflets, since the area changes have opposite signs, the area difference energy contribution is zero; on the other hand, if one holds lipid densities constant in each leaflet, one also regains the Helfrich Hamiltonian, albeit with different parameters. When considering area difference energy, it is between these two scenarios that one can expect deviations from the Helfrich.

Lipid flows. To be able to relax area difference, the membrane can change the lipid number asymmetry between leaflets. If one considers a region of membrane, barring local lipid consumption/production/adsorption, the balance of the number of lipids in each leaflet of the membrane can change in two ways. Lipids can flow in-plane, within the same leaflet, from the region boundary, where, for instance, the membrane can be connected to a lipid reservoir. Alternatively, there can be a net transmembrane flow of lipids from one leaflet to another. Both phenomena can then lead to a lipid asymmetry between leaflets. To be able to control the lipid asymmetry, in Eukarya living cells have transmembrane proteins called flippases that actively drive the transmembrane flow, and scramblases, transmembrane proteins that passively dissipate lipid asymmetry [44]. In fact any membrane border, such as those around membrane pores, can reduce lipid asymmetry by passively facilitating transit between leaflets by presenting a pathway that allows the lipid headgroups to remain in contact with the solvent. Lipids will also spontaneously and stochastically transit from one leaflet to another, flipping their orientation, in a phenomenon adequately named flip-flopping. The flip-flopping rate in relaxed membranes has been measured experimentally, and is usually reported to be a slow phenomenon for lipids, taking hours to days, but faster for other membrane components like cholesterol [37]. However, one might assume that significant area difference stress could force any of these transport methods to become more active compared to measurements done in relaxed membranes.

1.1.2 Measurement techniques in simulations

In order to study membrane reshaping at small curvatures, i.e. for phenomena where the deformations occur at many multiples of the membrane thickness, membranes are well described by the Helfrich Hamiltonian, and so by their bending modulus. There are multiple setups for determining it from simulations.

Membrane height fluctuation spectrum. When a tensionless flat membrane patch in periodic box of size L is placed into a thermal bath, the Helfrich can be rewritten in Fourier space, so that N^2 fluctuation modes develop, with $N = L/l$, where l is the membrane thickness. By the equipartition theorem each will acquire $k_{\mathrm{B}}T/2$ energy, from where one

derives that the amplitude of such a mode is linked to their wave vector $\vec{q}$ by:

$$\left\langle |h_{\vec{q}}|^2 \right\rangle = \frac{k_{\mathrm{B}}T}{L^2\kappa|\vec{q}|^4}$$

Thus by measuring their amplitudes and fitting this expression κ can be obtained [22].

Response to static deformation. Another option is measuring the return force of membrane forced into a static bent configuration [20]. When a flat membrane is compressed in one direction, it releases stress by buckling, and the return force is then connected to the bending cost of this buckling. The free energy can then be measured by thermodynamic integration over the degree of bending, and connected to the bending modulus via the Helfrich hamiltonian. In these methods, shape fluctuations are undesirable since they introduce noise that is both expensive to eliminate statistically, and effectively results in a static deviation from the intended configuration. These fluctuations scale with system size, thus there is a balance to be stricken between minimizing noise versus possible finite size effects.

Budding and topological changes. If one is concerned with topological changes, then the gaussian term becomes relevant. One method to determine the gaussian curvature modulus is to measure the probability of complete closure starting at different stages of the transition from flat patch to vesicle [31]. Another method is to simulate the adhesion, wrapping and budding of a spherical particle by a flat membrane patch under zero tension. The topology change should result in an energy difference involving both the bending modulus κ and the gaussian modulus $\bar{\kappa}$ [31]:

$$\Delta E_{\mathrm{budding}} = 4\pi\left(2\kappa + \bar{\kappa}\right) \tag{1.5}$$

By equating it with a critical adsorption total energy, with κ known from other measurements, it is possible to deduce $\bar{\kappa}$; however a possible complication is the existence of a barrier to the process, which should be possible to estimate from existing theory for the wrapping of colloids [18].

Stretching and forced pore formation. Membrane tension Σ can be determined by measuring the return force of a flat patch of membrane being stretched in periodic horizontal boundary conditions; at sufficient tension this results in the formation of a pore and tension is released. Both phenomena can be jointly analysed to determine the line tension λ together with the harmonic extensibility modulus M [17].

CHAPTER 2

Bolalipid membrane structure and mechanics

In this chapter, we introduce and define our model for archaeal membranes (Section 2.1), characterize its phase behaviour (Section 2.2), and split our analysis of their mechanical properties between pure bolalipid membranes (Section 2.3) and bilayer lipids / bolalipids mixtures (Section 2.4). We discuss the main findings in (Section 2.5). For the interested reader we go over the details of fluctuation spectrum analysis used to characterize both of these membrane types (Section 2.6).

2.1 Computational Model

To study bolalipid membranes and compare them to bilayers, we extended the Cooke and Deserno model for bilayer membranes [17]. In the original model for the bilayer a single bilayer lipid is represented by a chain of three nearly equally sized beads of diameter of $\sim 1\sigma$, where σ is our distance unit and roughly maps to $1\,\mathrm{nm}$ (Fig. 2.1A left); one bead stands for the head group (cyan) while the others represent the hydrophobic tail (blue). Each adjacent pair of beads in a lipid is linked by a finite extensible nonlinear elastic (FENE) bond. The angle formed by the chain of three beads is kept near 180° via an angular potential with strength k_0. While lipid heads interact exclusively through volume exclusion, the beads of lipid tails interact via a soft attractive potential of the strength ϵ_p and range ω (Fig. 2.1A left), effectively modelling hydrophobic interaction in an implicit solvent. This interaction strength governs the membrane phase behaviour and can be interpreted as the effective temperature $T_\mathrm{eff} = k_\mathrm{B}T/\epsilon_\mathrm{p}$.

To model a bolalipid molecule, we joined two bilayer lipids so that a lipid molecule is formed with a head bead (cyan) that is linked to four tail beads (crimson) which are again linked to another head bead (Fig. 2.1A right). In this way, both bilayer lipids and bolalipids share the same molecular structure and the same interactions between lipid beads. Bolalipids in archaeal membranes can differ in the number of cyclopentane rings or the branching of the tail and thus in the molecular stiffness [14, 15]. To represent this effect, we added two angular potentials between the second and the fourth and the third and the fifth tail bead with variable strength k_bola. By varying k_bola, we can control the molecular stiffness of the bolalipid molecules and thus model different types of bolalipids. The model is simulated within molecular dynamics implemented in the LAMMPS open source package [59], and simulations

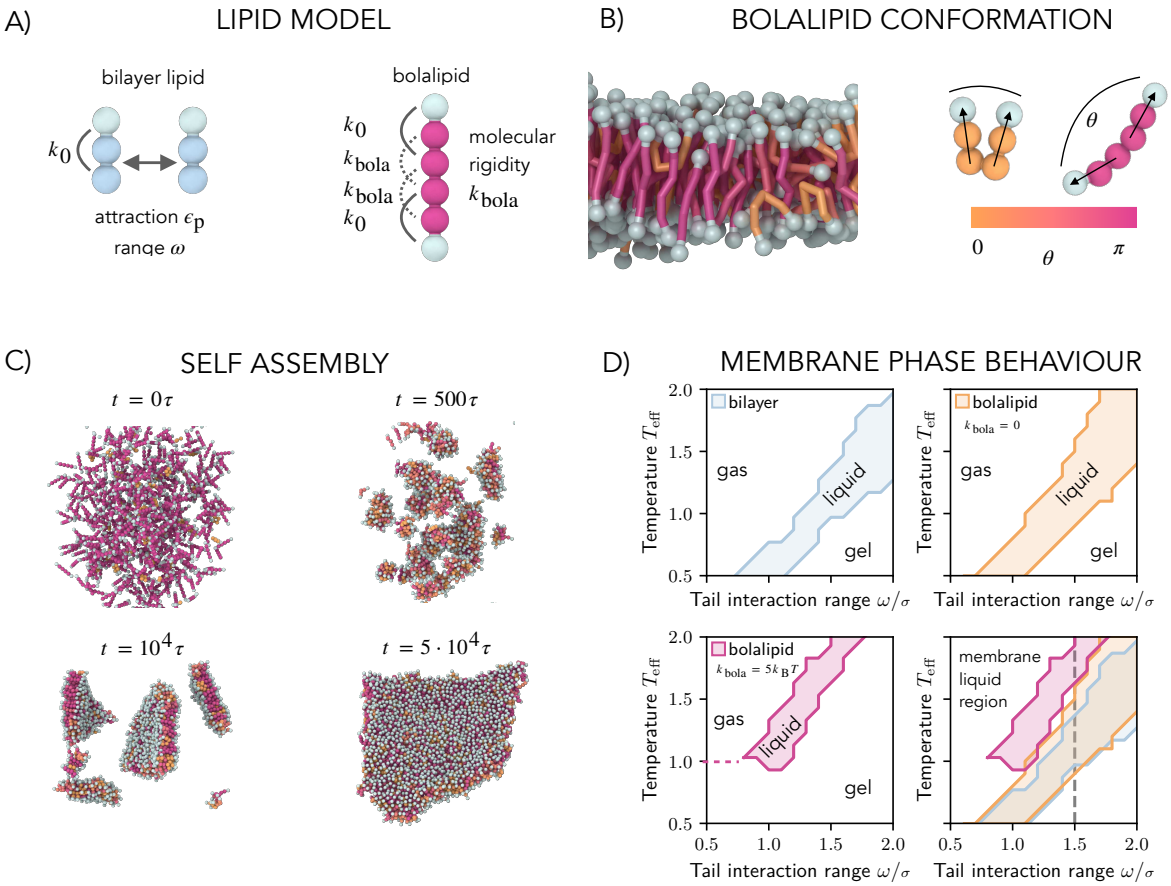

Figure 2.1: **Computational model and phase space of bilayer and bolalipid membranes.** (A) Bilayer lipid (left) is described with one head bead and two tail beads straightened by an angular potential of strength k_0. Tail beads of different lipids attract with the strength ϵ_p and the range ω. Bolalipids (right) consist of two bilayer lipids connected by a bond and straightened by an angular potential of strength k_{bola}. (B) Snapshots of bolalipids self-assembling into a flat membrane ($k_{bola} = 0.3\, k_B T$). (C) Cross-section of self-assembled membrane (right), with bolalipids coloured according to their conformation: straight lipid in crimson and U-shaped lipid in orange. (D) Membrane phase behaviour: liquid, gel and gas regions as a function of the effective temperature T_{eff} and tail interaction range ω for bilayer (top left) and membranes made of flexible $k_{bola} = 0$ (top right) and stiff $k_{bola} = 5\, k_B T$ (bottom left) bolalipid molecules. Overlays of all liquid regions (bottom right) show that stiffer lipids exhibit fluid membrane region at higher temperatures. The dashed line marks $\omega = 1.5\sigma$, the value we used in the rest of the work.

are visualized with OVITO [56]. We provide a LAMMPS input script generator, with examples of output, for simulating a flat patch of membrane at [2]. To include the implicit effect of the surrounding water and to simulate membranes at vanishing tension, we used a Langevin thermostat combined with a barostat that kept the membrane in the x-y plane at zero pressure. In the next subsection, we detail the potentials used for the bonds, angles and pair interactions mentioned above.

2.1.1 Implementation details

Each adjacent pair of beads in a lipid is connected by a finite extensible nonlinear elastic bond (FENE). For a given bond length r, its potential is the sum of an attractive term and a purely repulsive Lennard-Jones potential that enforces volume exclusion

$$U_{\text{bond}}(r) = -\frac{1}{2} K R_0^2 \ln\left(1 - \left(\frac{r}{R_0}\right)^2\right) + U_{\text{lj}}(r), \quad r \in [0, R_0] \tag{2.1}$$

with $K = 30 k_{\text{B}} T/\sigma^2$ and maximum length $R_0 = 1.5\sigma$ in the first term. We note that in the simulations our time, distance and energy units are respectively τ, σ and $k_{\text{B}} T$, and the Boltzmann constant $k_B = 1$. Consequently, our unit of mass is given by $1m = 1 k_{\text{B}} T \tau^2/\sigma^2$. The second term of Eq. (2.1) is given by

$$U_{\text{lj}}(r) = U_{\text{m}} \cdot \left(x^{-12} - 2x^{-6} + 1\right), \; x = \min(r, r_{\text{c}})/r_m \tag{2.2}$$

where r_m is where the potential reaches its minimum value U_{m} and r_{c} is its cutoff. For bonded beads, we set $U_m = 1 k_{\text{B}} T$, $r_{\text{m}} = r_{\text{c}} = 2^{1/6}\sigma$, so that the repulsive part is zero for $r > r_{\text{c}}$.

For non-bonded beads, as a first term we pick also a purely repulsive form with $r_{\text{m}} = r_{\text{c}} = 2^{1/6}\sigma \approx 1.12\sigma$, and parametrize on its strength by scanning the interval $U_{\text{m}} = \epsilon_{\text{p}} \in [0.5, 2] k_{\text{B}} T$. The inverse of this potential depth is the effective temperature $T_{\text{eff}} = k_{\text{B}} T/\epsilon_{\text{p}}$ in our system. Following Cooke and Deserno [17], we scaled down $r_{\text{m}}, r_{\text{c}}$ by 0.95 for interactions with head beads, to ensure no spontaneous curvature in a membrane leaflet [17],[31]. Accordingly, we note that in our snapshots each head bead is represented as a sphere of diameter 0.95σ and each tail bead as a bead of diameter 1σ.

To model lipid rigidity between each consecutive three beads b_1, b_2, b_3 in a lipid we set a harmonic angle potential

$$U_{\text{angle}}(\alpha) = K \cdot (\alpha - \pi)^2, \quad \alpha \in [0, \pi] \tag{2.3}$$

with $\alpha = \widehat{b_1, b_2, b_3}$. If one of the beads is a head bead (i.e. in a bilayer lipid), we set $K = k_0 = 5\, k_{\text{B}} T$. In contrast, for the two inner angles in a bolalipid we set the interval $K = k_{\text{bola}}$, where k_{bola} is a global constant in the simulation, equal for all bolalipids. In our work, for different simulations, we vary it in the interval $[0, 5] k_{\text{B}} T$. Therefore, the difference between a bolalipid and two bilayer-forming lipid molecules is the extra bond and two equal angle potentials keeping each three bead connected and aligned, respectively.

To model the (implicit) hydrophobic interaction between lipid tail beads, we add a longer range attractive cosine squared potential

$$\begin{aligned} U_{\text{cs}}(r) &= -\epsilon_{\text{p}} \cos^2\left(\frac{\pi}{2} \text{clip}\left(\frac{r - r_c}{\omega}, 0, 1\right)\right) \\ &= \begin{cases} -\epsilon_{\text{p}} & r \le r_c \\ -\epsilon_{\text{p}} \cos^2\left(\frac{\pi}{2}\frac{r - r_c}{\omega}\right) & r_c < r < r_c + \omega \\ 0 & r \ge r_c + \omega \end{cases} \end{aligned} \tag{2.4}$$

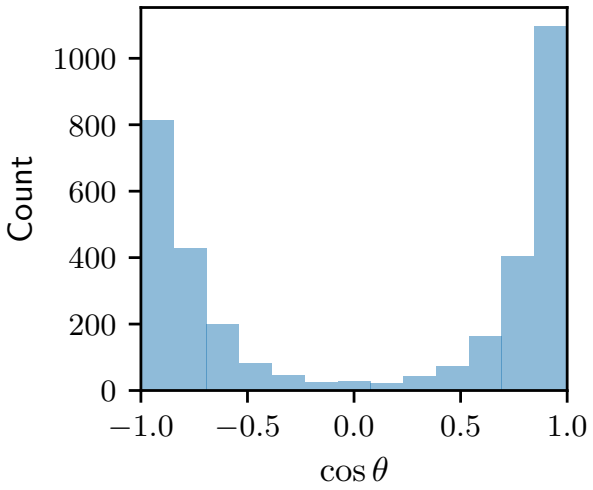

Figure 2.2: Histogram of the cosine of the angle θ between halves of a bolalipid ($k_{\text{bola}} = 0$) for the last frame of the simulation of a flat membrane of flexible bolalipids.

where $\text{clip}(x, a, b) = \max(\min(x, a), b)$ and r_c is set to the cutoff $2^{1/6}\sigma$ of the volume exclusion interaction. The repulsive Lennard-Jones and the attractive potential are combined to make the tail-tail interaction repulsive in the range $[0, r_c]$ and attractive in the range $[r_c, r_c + \omega]$. We take ω, the attractive range width, as a parameter. As we joined two bilayer lipids to form a bolalipid, in our model bilayer lipids and bolalipids share the same hydrophobic interaction.

2.2 Self-Assembly & Phase behaviour

Membrane self-assembly. While we expected bilayer membranes to self-assemble as documented in [17], we had to test if the same was true of bolalipid molecules. To do so, we placed dispersed lipids in a periodic 3D box. We start with an energy minimization that corrects non-physical configurations by slightly altering the particles positions. We then evolved the system with timestep $\delta t = 0.01\,\tau$ under a Langevin thermostat with relaxation time of 1τ and checked a flat membrane patch eventually formed (see Fig. 2.1B and Movie 1). In practice, unless the number of lipids and box dimensions were specifically tuned, we obtained several isolated patches of membrane, which in some long simulations eventually merged into a single flat patch, not necessarily aligned with the box horizontal plane.

Bolalipid in-membrane conformations. For small enough values of k_{bola}, single lipids are flexible and can thus adopt a range of possible conformations. The different conformations can be classified by the angle θ between the two lipid heads (Fig. 2.1C). Specifically, if the beads in a bolalipid are numbered $b_1, .., b_6$, from head to head, $\theta = \angle\overrightarrow{b_3, b_1}, \overrightarrow{b_4, b_6}$. Two lipid conformations dominated the conformation distribution in the context of a membrane: the U-shaped conformation with both head beads on the same membrane leaflet ($\theta \approx 0$) and the straight conformation with one head bead in opposing membrane leaflets ($\theta \approx \pi$) (Movie 2.b and Fig. 2.2; for comparison, bilayer membranes in Movie 2.a and rigid bolalipid membranes in Movie 2.c). In the self-assembled bolalipid membrane, we marked bolalipids as being in the U-shape conformation if $\theta < \pi/2$ and in the straight conformation otherwise.

2.2.1 Setup & Analysis

Membrane pre-assembly. To shorten the runtime of our membrane simulations and to ensure an intended initial shape and topology, like a single horizontal flat patch, we pre-assemble the membrane. This is done by discretizing the membrane into two vertically aligned horizontal hexagonal grids, separated by half the expected membrane thickness, and with roughly the correct spacing for a provided area per lipid head. For bilayer membranes, a lipid is then placed at the centre of each hexagonal cell. This was sufficient: after an initial energy minimization, the system is cohesive enough to withstand thermalization. For bolalipid membranes, we first proceed assuming that at equilibrium the two conformations would follow a two state model with energy difference ΔE computed directly from assuming the angles between the two central tail beads would be π for the straight conformation and $\pi/2$ for the U-shaped conformation. From this model we obtain an initial fraction of U-shaped bolalipids. To place bolalipids in the lattice, we initially found that successfully reducing overlap, via energy minimization, was overly parameter dependent. Instead, we increased the hexagonal grid dimensions, so we could place each lipid by itself on each vertical unit of the lattice, thus avoiding overlap; we then lock the lipids vertical position and conformation, compress with volume exclusion until the target area per head is reached, perform energy minimization, and check that the lipids form a horizontal single cluster.

Near-zero tension ensemble. After pre-assembling flat membranes, we combined the previously used Langevin thermostat with relaxation time of 1τ with a NoséHoover barostat with relaxation time of 10τ. In LAMMPS this amounts to combining the commands 'fix langevin' with 'fix nph'. We configured the barostat to set lateral pressure P_{xy} to zero by re-scaling the simulation box in the x-y plane. This effectively gives rise to an NPT ensemble, where, as long as the membrane remains relatively flat, membrane tension is kept zero.

Membrane Stability. We tested the stability of both bilayer and bolalipid membranes over a wide range of parameters. For determining membrane stability, we pre-assembled as described before a flat membrane patch so that we had roughly 25^2 head beads in each leaflet. Equivalently, this amounted to roughly 1250 bilayer lipids or 625 bolalipids, for single-species membranes. For sufficiently high T_{eff}, we expect lipids to evaporate into a gas phase, leading to large pore formation, the membrane splitting into separate patches, and eventually the simulation box size diverging as the barostat tries, to no avail, to keep the lateral pressure from increasing; therefore we set up our simulation so it would automatically halt if the simulation box size became twice its starting value. We mark the membrane as being in the gas phase if we observe either the early signs of membrane instability or the full disassembly. If the membrane otherwise remains stable, we ran the simulation to completion for $\Delta_{\mathrm{total}} = 10 \times 10^3\,\tau$. This was determined to be sufficient for both the box size L and the relative amounts of lipid conformations to equilibrate.

Measuring Diffusion. We then analysed the diffusion of single lipids for the stable membranes. For computing the diffusion constant D, we first found the corresponding mean square displacement for each Δt and then fitted $D = \langle|\Delta x|\rangle / (\Delta t)$. To compute the M.S.D. of a specific lipid in a temporary conformation, we averaged $|\Delta x|$ over all possible intervals of duration Δt where the conformation was held. We took care to exclude displacements of lipids floating in the gas phase of the simulation.

2.2.2 Results

The diffusion constant D exhibited a discontinuity as a function of the temperature T_{eff}, which marks the transition as the membrane moves from the gel phase to the liquid phase. The discontinuity occurred at different values of interaction strength ϵ_{p} and interaction range ω for bilayer and bolalipid lipids, and it also depended on the values of the molecular stiffness k_{bola} (Fig. 2.3). Fortunately, for all membranes and parameters tested the gel membranes and the liquid membranes could be separated by simple rule of setting the threshold for liquid phase at $D \geq 5 \times 10^{-4}\,\sigma^2/\tau$. In these simulations, the disintegration of the membrane defined an upper limit in T_{eff} to the liquid phase and the transition to the gas phase. Based on this classification, we plotted the phase diagram for bilayer membranes (Fig. 2.1D top left), fully flexible bolalipid membranes ($k_{\mathrm{bola}} = 0$, Fig. 2.1D top right), and rigid bolalipid membranes ($k_{\mathrm{bola}} = 5\,k_{\mathrm{B}}T$, Fig. 2.1D bottom left) as a function of the range of the hydrophobic interaction ω and the temperature T_{eff}. Membranes made of bilayers (blue) and flexible bolalipid molecules ($k_{\mathrm{bola}} = 0$, orange) behaved similarly under these conditions (Fig. 2.1D bottom right). Strikingly, just as observed in extremophile archaea, as the molecular stiffness of bolalipids increased ($k_{\mathrm{bola}} = 5\,k_{\mathrm{B}}T$, magenta), the liquid region was shifted toward higher temperatures and larger values of the interaction range. This is possibly due to the fact that bolalipid molecules are able to engage in more extensive interactions with partners when in the extended conformation, which helps to stabilize the membrane at higher temperatures.

Going from bilayer membranes to rigid bolalipid membranes, the gel to liquid phase transition corresponds to an increase of T_{eff} by a factor from 2 to 1.7 as ω is increased. A simple explanation can be made based on entropy alone. At the transition effective temperature $T_{\mathrm{eff}}^{\mathrm{melt}}$ from gel to liquid the loss in packing energy must be the same as the entropic gain, so we get $\Delta U = \Delta TS$. If we assume that the change, from gel to liquid, in average potential energy ΔU is mostly contributed by the pair potential interactions, that determine the packing of lipids, then we get that $\Delta U = \beta/T_{\mathrm{eff}}$, where β depends only slightly on the membrane type t and the interaction range ω. Since we have constant T (not T_{eff}) we then expect the transition temperature $T_{\mathrm{eff}}^{\mathrm{melt}} \propto 1/\Delta S$. In the gel phase, we assume the lipids are packed well enough that the entropy per bead is similar for all types of membranes. In a liquid bilayer system, if N states are available in a single leaflet, then N^2 are available in total, and so the translational entropy is $2\log N$. On the other hand, a liquid monolayer system such as a rigid bolalipid membrane is equivalent to a single leaflet and so has entropy $\log N$. Consequently, $T_{\mathrm{eff}}^{\mathrm{melt}}$ follows the inverse ratio, with the melting temperature of rigid bolalipids being twice that of the bilayer. As for the flexible bolalipids, their membranes likely recoup the entropic cost of being partially a monolayer by having two conformations available to each lipid, and thus have the same melting temperature as a bilayer system.

2.3 Bolalipid conformations and mechanical properties

To explore mechanical properties of bolalipid membranes, we chose $\omega = 1.5\,\sigma$ for the remainder of the work (dashed line in Fig. 2.1D bottom right). Fig. 2.4A shows the phase diagram for bolalipid membranes replotted as a function of temperature and bolalipid rigidity for the chosen interaction range. To be able to compare membranes made of bolalipids of different molecular rigidities, we needed to adjust temperature for each to reach similar fluidities, shown by dashed lines in Fig. 2.4A. We then characterized the conformations of individual bolalipids in flat membranes, measured by the fraction of bolalipids in U-shape conformation u_{f}. We find that for flexible bolalipids ($k_{\mathrm{bola}} = 0$), more than 50% of all lipids are in the U-shape conformation

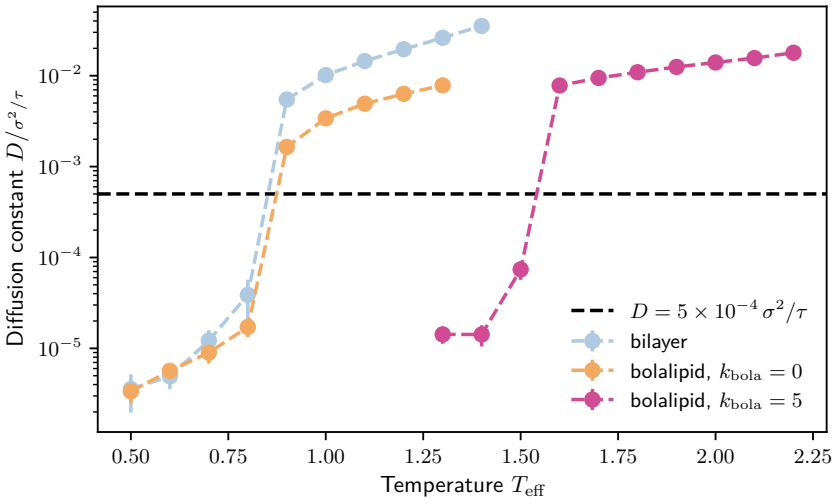

Figure 2.3: Diffusion constant for different pure membranes at $w = 1.5\,\sigma$ versus temperature T_{eff}. The discontinuity (jump) in D marks the transition from the gel phase to the liquid phase. The dashed black line marks the minimum diffusion constant that is required to classify as a liquid membrane at $D = 5 \times 10^{-4}\,\sigma^2/\tau$.

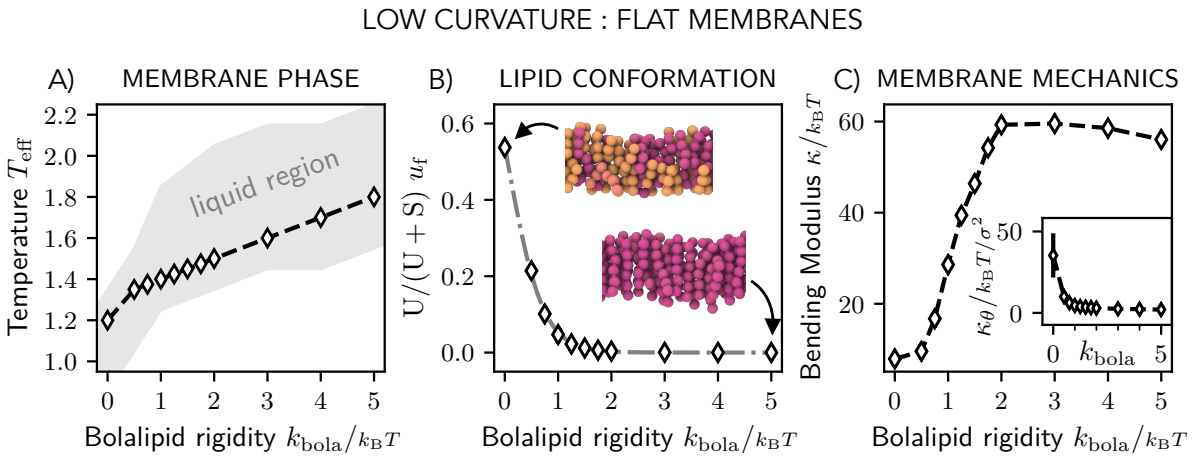

Figure 2.4: **Mechanics of pure bolalipid membranes.** (A) Liquid region as a function of temperature and bolalipid rigidity for pure bolalipid membranes (grey). The dashed line shows the bolalipid membranes of approximately same fluidities. (B) Fraction of bolalipids in the U-shape conformation ($\theta = 0$), fitted to $u_{\mathrm{f}}(k_{\mathrm{bola}}) = 1/(1 + \exp(\beta(-0.16 + 3k_{\mathrm{bola}})))$ (grey dashed line) according to a two-state model. Insets: simulation snapshots with bolalipids coloured according to their conformations. (C) Bending modulus as a function of bolalipid molecule rigidity k_{bola}. Inset: Tilt modulus as a function of bolalipid rigidity k_{bola}.

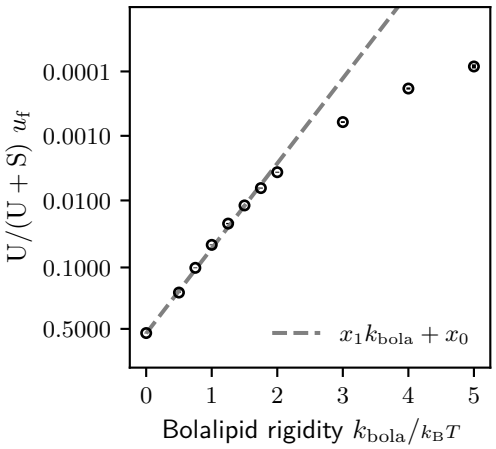

Figure 2.5: Data and fit to U-shape fraction in pure bolalipid membranes, in transformed coordinates $y = \log\left(\frac{1}{u_f} - 1\right)$ that allow fitting the y values with a linear expression. For $k_{bola} \leq 2k_B T$, measurements of the U-shaped bolalipid fraction had less than 1% relative error, so error bars are barely visible. More importantly, given that simulations above this threshold contained on average less than a single U-shape bolalipid, we judged the fit based on the R^2 value considering only the points below $k_{bola} \leq 2k_B T$, for which get $R^2 = 0.99$.

(Fig. 2.4B). This fraction decreases with increasing rigidity of bolalipid molecules and vanishes around $k_{bola} \geq 2\, k_B T$, for which almost all bolalipids take up linear conformations.

Modelling conformation statistics. This behaviour can be easily captured by considering bolalipids as a two state system, with straight and U-shape conformation, as argued before (Fig. 2.2). We express the difference between the free energy of a U-shaped and a straight shaped conformation as $E_u - E_s = c_0 + c_1 k_{bola}$, that is, a first order approximation on k_{bola}. The fraction of bolalipids in U-shape conformation then follow $u_f(k_{bola}) = 1/(1 + \exp(\beta(c_0 + c_1 k_{bola})))$, with $\beta = 1/(k_B T)$, as shown by the fit in Fig. 2.4B (dashed grey line). We judged our the fitness of our model by first making it linear, expressing it as $\log(1/u_f - 1) = x_1 k_{bola} + x_0$; then we restricted it to points where $k_{bola} \leq 2\, k_B T$, or, equivalently, when there were on average ≈ 2 or more U-shaped bolalipids; with these choices we obtained $R^2 = 0.99$ (Fig. 2.5).

For the fit we get $c_1 = 3$ and $c_0 = -0.16 < 0$, which implies that bolalipids in U-shape conformation are slightly favoured over straight bolalipids at $k_{bola} = 0$. These factors are definitely different from the ones for the first principles initial configuration formula, for which $c_0 = 0$ and $c_1 = 2(\pi/2)^2 \approx= 4.9$. That the final configuration is different from the initial is fortunate, since, having already checked u_f is equilibrated and not slowly changing, we are also sure the change is not so small that it would be undetected by our equilibration criteria. This equilibration can be seen by eye in Fig. 2.6, happening in the first 1000τ's. Since however this means equilibration for the chosen initial values happened strictly by increasing the amount of U-shaped conformers, to confirm the opposite was possible we also ran simulations where we started the membrane solely with U-shaped bolalipids, or solely with straight bolalipids, at $k_{bola} = 0$; in the first case we confirmed the U-shape fraction shrunk to the equilibrium value in less than $10 \times 10^3\, \tau$ (Fig. 2.7).

Bolalipid conformations and membrane rigidity. It was previously hypothesized that an increasing fraction of bolalipids in straight configuration would increase the membrane rigidity

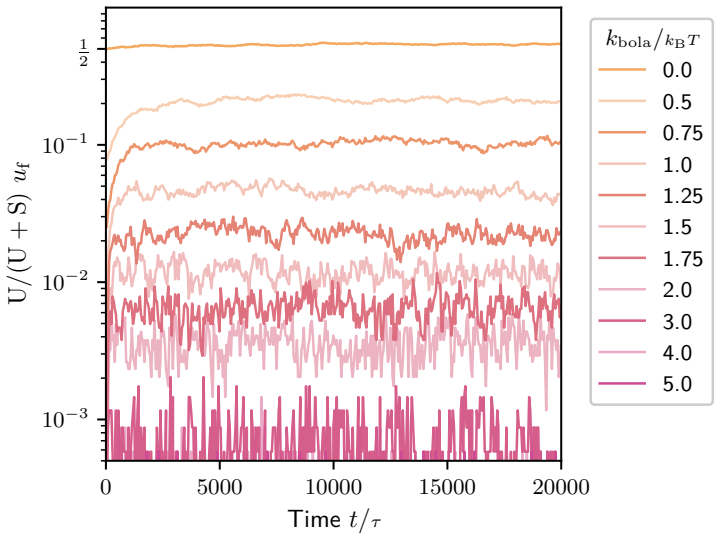

Figure 2.6: Time series of fraction of bolalipids in the U-shaped conformation u_f, for simulations of pure bolalipid membranes with different values of the bolalipid rigidity k_{bola}.

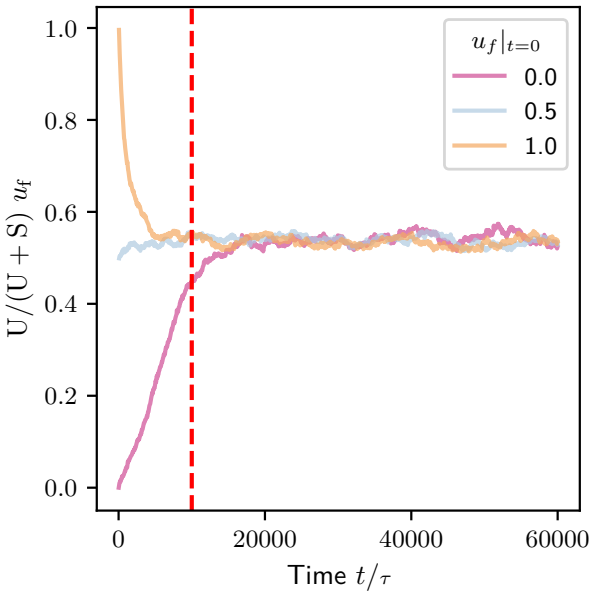

Figure 2.7: Time series of u_f, the fraction of bolalipids in the U-shaped conformation, for the simulations done for flexible bolalipids ($k_{\mathrm{bola}} = 0, T_{\mathrm{eff}} = 1.2$), where the system was pre-assembled with three different initial values $u_f|_{t=0}$. The red dashed line marks the joint equilibration time of $10 \times 10^3\,\tau$.

[62]. To determine the membrane rigidity using our model, we assessed the height fluctuation spectrum (h^2) of flat membranes in a periodic box. [17, 38]. Interestingly, we found that the original theory of Helfrich [29] failed to describe the resulting height fluctuation spectrum (see Section 2.6). However, the extended theory by Hamm and Kozlov [27], which also includes the energetic cost of lipid tilt, successfully captured bolalipid fluctuations. In this case, the resulting height spectrum of the membrane at vanishing membrane tension is given by [38]

$$\begin{aligned}\langle |h_n|^2 \rangle &= \frac{k_\mathrm{B}T}{L^2}\left(\frac{1}{\kappa q^4} + \frac{1}{\kappa_\theta q^2}\right) \\ &= \frac{k_\mathrm{B}T}{L^2}\frac{1}{\kappa}\left(\frac{1}{q^4} + \frac{l_\theta^2}{q^2}\right), \end{aligned} \tag{2.5}$$

where $q = 2\pi n/L$ is the wave number, L is the box size, κ is the bending rigidity of the membrane, κ_θ is the tilt modulus and $l_\theta = \sqrt{\kappa/\kappa_\theta}$ is a characteristic length scale related to tilt. Considering Eq. (2.5), the tilt term is expected to matter if the analysed inverse wave numbers become similar to l_θ. The wave numbers that we analysed correspond to wavelengths that are at least twice the thickness of the membrane ($q < 2\pi/(12\sigma) \approx 0.5\,\sigma^{-1}$). Thus, the tilt term is expected to contribute if $l_\theta > 2\,\sigma$. For typical bilayer membranes, one finds $\kappa_\theta = 12\,k_\mathrm{B}\,T\,\mathrm{nm}^{-2}$ [38] and $\kappa = 20\,k_\mathrm{B}\,T$ [19], so $l_\theta \sim 1\,\mathrm{nm} \approx 1\,\sigma$ and therefore the tilt term can be neglected as practised before [17]. However, when the membrane rigidity increases as we expect for bolalipid membranes, l_θ increases and the tilt term in Eq. (2.5) becomes relevant.

By fitting the height fluctuation spectrum (see Section 2.6) for bolalipid membranes, we measured the bending rigidity (Fig. 2.4C) and tilt modulus (Fig. 2.4C inset) as a function of k_bola. With increasing bolalipid molecular rigidity k_bola, the bending rigidity κ rose from $8\,k_\mathrm{B}\,T$ and plateaued at $60\,k_\mathrm{B}\,T$, showing bolalipid membranes can be very rigid while liquid. Strikingly, the increase in membrane rigidity coincided with U-shaped bolalipids vanishing from the membrane (Fig. 2.4B), which confirmed the hypothesis that straight bolalipids render lipid membranes rigid. At the same time, the tilt modulus κ_θ decreased with bolalipid rigidity, from $30 \pm 10\,k_\mathrm{B}\,T/\sigma^2$ to $2\,k_\mathrm{B}\,T/\sigma^2$, lowering less than $1\,k_\mathrm{B}\,T$ for $k_\mathrm{bola} \geq 2\,k_\mathrm{B}\,T$. Since membrane bending and lipid tilting are two modes of membrane deformations that compete, we conclude that bilayer and flexible bolalipids molecules form flexible membranes that prefer to bend rather than to tilt, while bolalipids in straight configuration form rigid membranes that prefer to tilt rather than to bend.

By systematically investigating the membrane rigidity as a function of temperature T_eff, we found that in general flexible bolalipid membranes have a slightly increased rigidity compared to bilayer membranes (Fig. 2.8). We also found that by increasing T_eff, a rigid bolalipid membrane softens in the same manner as bilayer and flexible bolalipid membranes (Fig. 2.8).

Taken together, bolalipid membranes made of flexible lipid molecules are as flexible as lipid bilayers, adopting U-shaped conformations, where those made of bolalipids in straight configurations are rigid.

We note that for both the bilayer and the flexible bolalipid membrane, in $T_\mathrm{eff} \in [1.2, 1.3]$, the tilt modulus varies non-monotonically. It first increases, aligning with the expectation that higher pair potential temperature would reduce order and thus increase the cost of local coordinated tilting, i.e., increasing the tilt modulus κ_θ. However, at the higher T_eff it abnormally decreases. We attribute this to phase changes due to proximity to the liquid-gas transition. We also note that in our large flat membrane simulations ($L \approx 60\sigma$), flexible

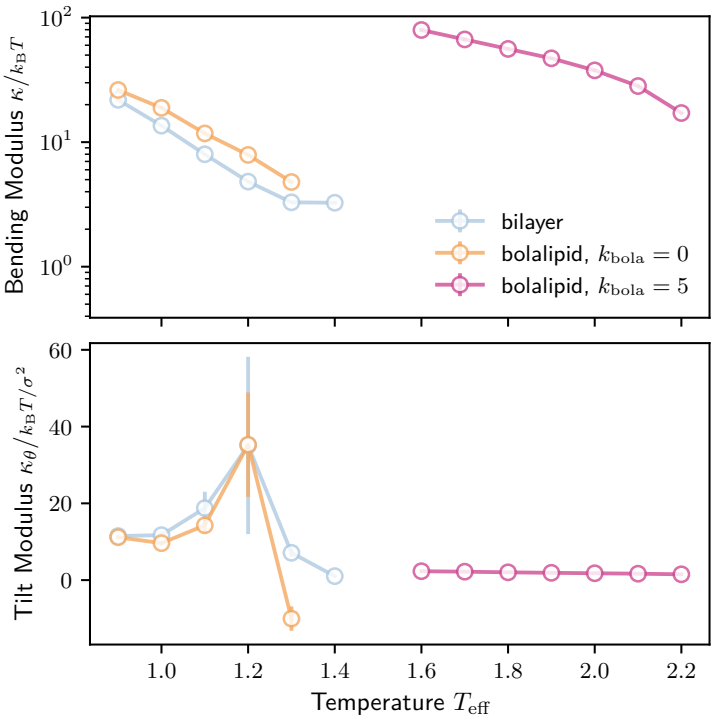

Figure 2.8: Fluctuation spectrum fit results, with (top) bending and (bottom) tilt modulus, for bilayer, flexible bolalipid and rigid bolalipid membranes at $w = 1.5$ as a function of T_{eff}.

bolalipid membranes at $\omega = 1.5\sigma$ are stable only at temperatures smaller than $T_{\text{eff}} < 1.4$. For $T_{\text{eff}} = 1.4$ and presumably above, the membrane folds while shrinking the box until self-contact occurs. On the other hand, both the bilayer membranes and rigid bolalipid membranes of same size disassemble by pore formation, followed by simulation box expansion in response to the increased pressure, respectively at $T_{\text{eff}} = 1.5$ and 2.3. This explains why in Fig. 2.8 we have data for bilayer at higher T_{eff} than for the flexible bolalipids.

Gaussian rigidity of bolalipid membranes. Another important material parameter is the Gaussian bending modulus $\bar{\kappa}$, which characterizes the reshaping behaviour of fluid lipid membranes under topological changes [19]. $\bar{\kappa}$ is notoriously difficult to measure since it only becomes detectable when the membrane changes its topological state. Continuum membrane theory, combining stability arguments and elasticity, predicts $-\bar{\kappa}/\kappa \in [-0.5, -1]$ [19], where the former value is expected for incompressible membranes. Indeed, most of the numbers we know for the ratio of the two bending rigidities, many of which were deduced from simulations, lie within this range [31]. Using the same method as developed by Hu et al. [31], we determined $\bar{\kappa}$ by measuring the closing efficiency of membrane patches into a sphere (see [3] for details). We obtained $\bar{\kappa} = -4.61 \pm 1.91\, k_B T$ and thus a ratio of $-\bar{\kappa}/\kappa = 1.07 \pm 0.50$ for bilayer membranes. In contrast, we got significantly larger values (less negative) with $\bar{\kappa} = -2.81 \pm 2.41\, k_B T$ and $-\bar{\kappa}/\kappa = 0.55 \pm 0.49$ for flexible bolalipid membranes ($k_{\text{bola}} = 0$). The result shows that in addition to the differences in bending rigidities, the ratio of the two bending moduli differs strongly in bilayer and bolalipid membranes.

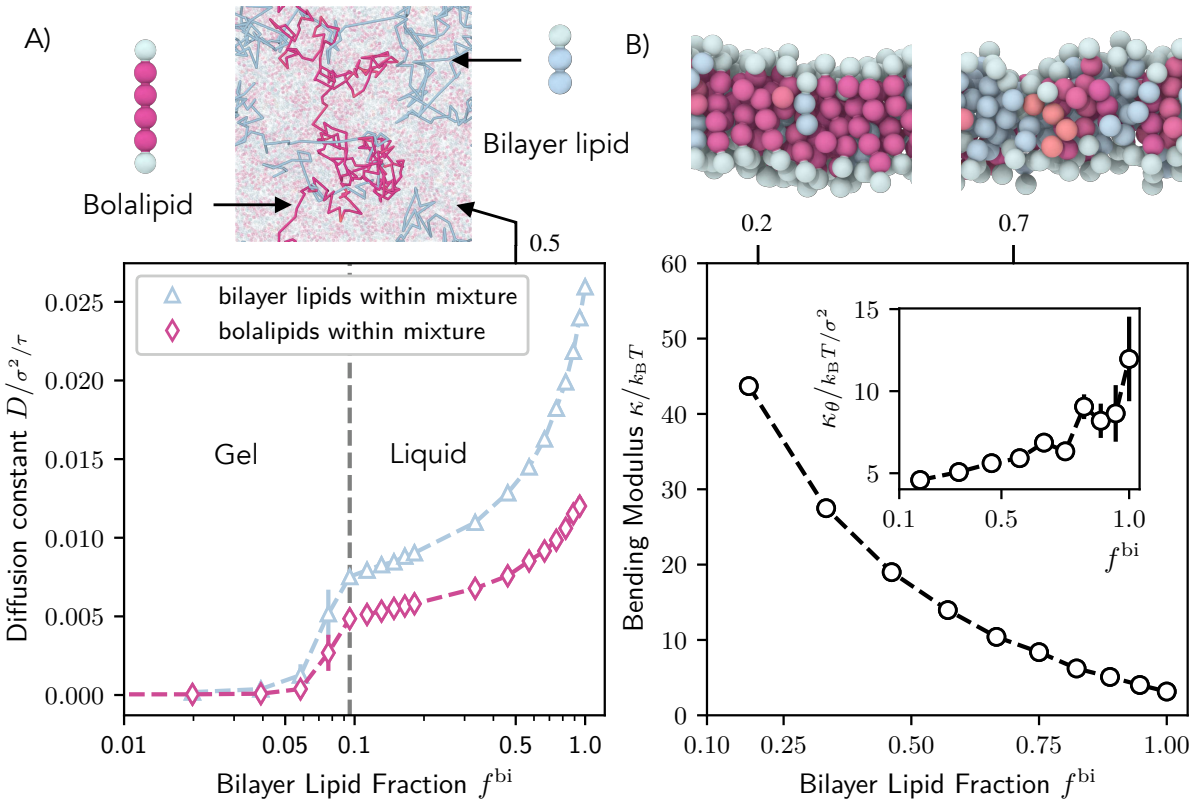

Figure 2.9: **Fluidity and rigidity of mixed bilayer/bolalipid membranes.** (A) Single lipid diffusion constant for each species as a function of bilayer lipid fraction f^{bi} (at $k_{\mathrm{bola}} = 2k_{\mathrm{B}}T$, $T_{\mathrm{eff}} = 1.3$). For $f^{\mathrm{bi}} \geq 0.1$, the resulting mixture becomes liquid. Top: Diffusion trajectories of a bolalipid (blue) and a bilayer lipid (red) in a mixture membrane at $f^{\mathrm{bi}} = 0.5$. (B) Bending rigidity κ and (Inset) tilt modulus κ_θ as a function of the fraction of bilayer molecules f^{bi}. Top: Snapshots show bilayer lipids (blue) in mixed membranes at two different values of f^{bi}.

2.4 Archaeal membranes made of mixtures of bolalipids and bilayer-forming lipids

Archaeal membranes contain varying amounts of bilayer lipids [41, 60]. The exact bolalipid/bilayer fraction depends on the growth temperature, with higher levels of bolalipids with increasing temperature [34], and higher fraction of cyclopentane rings in the tails [15]. In order to investigate the effect of different lipid contents on membrane mechanical properties, we wanted to model the archaeal membrane by mixing bilayer lipids into bolalipid membranes. Since in our model, the liquid regions of rigid bolalipid membranes and bilayer membranes do not overlap (Fig. 2.1F bottom right), we picked the temperature $T_{\mathrm{eff}} = 1.3$ to minimize fluidity mismatch, and we set the molecular rigidity $k_{\mathrm{bola}} = 2\,k_{\mathrm{B}}T$ to limit U-shaped bolalipids (Fig. 2.4B). We then measured the diffusion constant D as a function of the fraction of bilayer lipids f^{bi}. Interestingly, we found that mixing only 10% bilayer lipids into the bolalipid membrane in gel state is enough to fluidize the membrane (Fig. 2.9A). We then measured the bending rigidity and the tilt modulus of flat mixture membranes by analysing the fluctuation spectrum. While the bending rigidity κ decreased (Fig. 2.9B), the tilt modulus increased non-linearly with the bilayer lipid fraction f^{bi} (Fig. 2.9B inset). Taken together, the bolalipid membrane can be

substantially softened either through bolalipids acquiring U-shaped conformation or through addition of bilayer-forming lipids.

2.5 Discussion

In our model, bolalipids are formed by joining together two bilayer lipids, with an adjustable molecular stiffness at the hinge point. Using our model we find striking differences between bilayer and bolalipid membranes in terms of stability and rigidity.

While flexible bolalipid membranes are liquid under the same conditions as bilayer membranes, we found that stiff bolalipids form membranes that operate in the liquid regime at higher temperatures. These results agree well with previous molecular dynamics simulations that suggested that bolalipid membranes are more ordered and have a reduced diffusivity compared to bilayer membranes [12, 32]. In our simulations, this is due to the fact that completely flexible bolalipids molecules adopt both straight (transmembrane) and the U-shaped (loop) conformation with approximately the same frequency. In contrast, stiff bolalipids typically only take on the straight conformation when assembled in a membrane. These results agree with the previous coarse-grained molecular dynamics simulations using the MARTINI force field which showed that the fraction of straight to U-shaped bolalipids increased upon stiffening the linker between the lipid tails [12].

When we determined the bending rigidity of bolalipid membranes by measuring their response to thermal fluctuations, we found that membranes made from flexible bolalipids are only slightly more rigid than bilayer membranes. This result is consistent with previous atomistic simulations, which showed that the membrane rigidity was similar for membranes composed of bilayer lipids and flexible synthetic bolalipids [51]. Moreover, the result is consistent with a continuum theory which predicted that the rigidity of membranes formed of triblock copolymers is 20% larger than that of diblock copolymers [64]. However, bolalipids in extremophilic archaea are not predicted to be fully flexible as they are expected to pack tighter due to a large number of cyclopentane rings in the lipid tails [14, 15]. Indeed, we found that membranes made of stiff bolalipid molecules can exhibit stiffness that is more than an order of magnitude larger than that of bilayer lipids at the same membrane fluidity.

A marked difference between bilayer and flexible bolalipid membranes is that the Gaussian bending rigidity is that the ratio of Gaussian rigidity to the bending modulus is around $1/2$, instead of the usual for bilayers ≈ 1. It is not obvious how the Gaussian bending modulus would behave upon increasing bolalipid stiffness ($k_{\mathrm{bola}} > 0$), but it should be possible for not too high values of k_{bola}.

It is interesting to draw a parallel between monolayer membranes made of stiff bolalipid molecules and macroscopic membranes composed of rigid straight colloidal particles, which are geometrically similar, but living at different scales [21]. Furthermore, it has been found that colloidal membranes at these macroscopic scales follow the standard Helfrich theory for bilayer membranes [7], with rigidity that is three orders of magnitude higher than those of lipid bilayers [6]. In this case the tilt modulus was not pertinent, likely due to macroscopic system sizes. Similarly, we expect that the bending rigidity can be determined from membrane fluctuations independently of the tilt modulus for bolalipid membranes if they are prepared at similar relative sizes.

We found that membranes formed of a mixture of bilayer and bolalipids, similar to archaeal membranes, function as a composite liquid membrane that softens when adding bilayer lipids.

However, while in our simulations the bending rigidity monotonically decreases with bilayer fraction, previous experiments of mixture membranes of bilayer and bolalipids with cyclopentane rings suggested that the bending rigidity non-monotonically depends on the fraction of the membrane made up of bilayer lipids [62]. It remains to be determined whether the result is due to the specific lipids used, the resulting mismatch in lengths between two stacked bilayer lipids and a straight bolalipid, the experimental conditions or to non-linear effects such as the formation of lipid domains that soften the membrane with increasing bolalipid content. The same experiments reported that membranes consisting solely of bolalipids are more rigid than bilayer membranes and non-fluctuating, which is in agreement with our high bending modulus simulation results for near-pure bolalipid mixture membranes.

2.6 Fluctuation spectrum protocol & analysis

To determine the membrane rigidity using our model, we assessed the height fluctuation spectrum (h^2) of flat membranes in a periodic box. [17, 38].

Simulation setup. In order to measure height fluctuation spectrums (Fig. 2.4C, and Fig. 2.9B), we used membranes with 60^2 head beads per leaflet, with minimum Δ_{eq} set to $20 \times 10^3 \tau$; total runtime was $\Delta_{\mathrm{total}} = 60 \times 10^3\, \tau$. We note that the long runtime was needed to obtain acceptable measurement errors; this is because the most relevant modes for this method are those with wavelength far above the membrane thickness or equivalently with low wavenumber q, and that for this implicit solvent model the relaxation time of a mode scales as q^{-4} [17]. We simulate a horizontal membrane in a periodic simulation box of dimensions $(l_{\mathrm{x}}, l_{\mathrm{y}}, l_{\mathrm{z}})$, that is horizontally square with $l_{\mathrm{x}} = l_{\mathrm{y}} = L$. Importantly, we keep membrane tension to a minimum by setting the lateral pressure $P_{\mathrm{xx}} = P_{\mathrm{yy}} = 0$ via a barostat.

As a first equilibration check, we consider the lateral box size L time series. Starting by considering the full series, we measure how much the first and last half differ. For each half, we compute the maximum, minimum and the diameter (max - min). If the relative difference is less than 30%, we consider it equilibrated. Otherwise, we exclude the first frame of the time series, and repeat the check.

Height field spectrum measurement and ensemble averaging. For each of the N_{f} remaining frames, we intend to obtain the height field of the membrane $h(x, y)$ within the x-y plane. However, our simulations are particle-based and hence our system is discrete. Therefore, we divide the horizontal plane in a regular $m \times m$ grid, where m is the length of a grid cell. We set $m = 40$ by trial and error so that no bins will be empty. Then we compute h_b, the average height of bin b. Finally, we apply the 2D discrete Fourier transform in the x-y plane, obtaining complex components h_n for $n \in [-m/2, ..., 0, .., m/2] \times [-m/2, ..., 0, .., m/2]$, with $h_n = h_{-n}$.

We correct for the binning by multiplying by $\mathrm{sinc}(n_x/m)\,\mathrm{sinc}(n_y/n)$, which mostly affects the smallest wavelengths [17]; we also scale by $\langle L \rangle$ obtaining $u = h\langle L \rangle$. For each wavenumber vector $n = (n_x, n_y)$ of u, we compute its amplitude squared $|u_n|^2$ and phase $\angle u_n$ (examples in Fig. 2.10). For both the amplitude and phase we then compute the autocorrelation time τ_c in order to get the statistical inefficiency $g = 2\tau_c + 1$. The phase should regularly jump through the endpoints $[0, \pi]$, so checking it too for stationarity allows excluding modes whose amplitude is static but which have their phase stuck. By doing this, we find that we can improve the analysis compared to the current state of the art [22], which only checks the

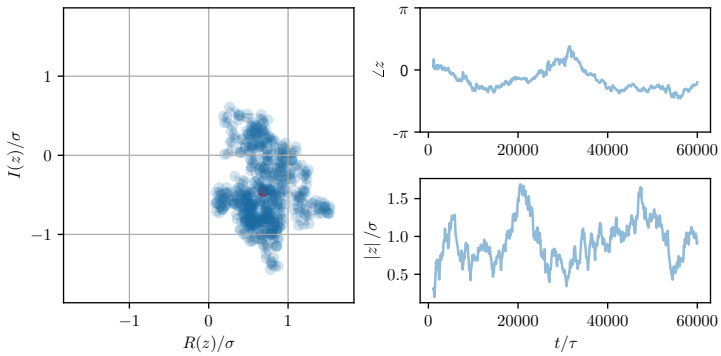

(A) non-equilibrated mode at $n = (1, 0)$.

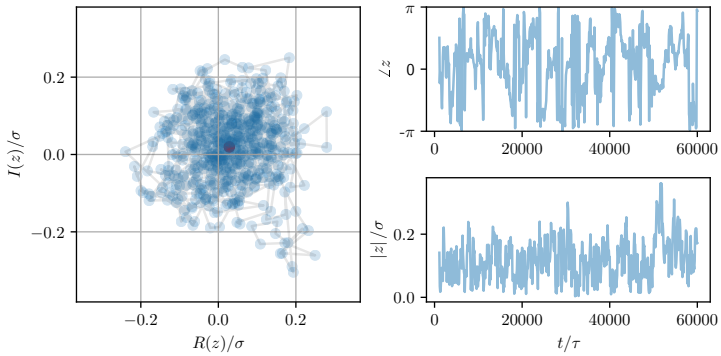

(B) equilibrated mode at $n = (2, 0)$.

Figure 2.10: Path of the complex component of the fourier transform of membrane height at $n = (1, 0)$ (A) and $n = (2, 0)$ (B) for bolalipid pure membrane at $k_{\text{bola}} = 0.5 k_{\text{B}} T$. Left plots show the trajectory in the complex plane, while on the right we plot their phase and norm versus time. The mode in (A), with an autocorrelation time of roughly $10^4\tau$, has only 10 uncorrelated points. On the other hand the mode in (B), with an autocorrelation time of approximately $10^3\tau$, has ≈ 60 uncorrelated samples and thus crosses the chosen threshold of 20 samples for being considered equilibrated.

amplitude squared. Between both the amplitude squared and phase components, we take the largest g, which then gives us the number of uncorrelated data points as N_{f}/g. We accept a mode as equilibrated if the remaining trajectory contains at least 20 uncorrelated data points. The standard deviation of the mean of $|u_n|^2$ must then be scaled by $\sqrt{g}$. For each spectrum measurement, we performed four simulations with different seeds for the thermal noise. We retained only modes which had equilibrated on all replicas and averaged over modes with the same wavenumber. We checked that the box size L varied less than 1% between replicas. To not impose an artificial variable window in wavenumber, we computed the first equilibrated mode for all our simulations and took the maximum equilibrated wavenumber as a global minimum threshold. We found in our simulations $n \geq 2$. This roughly corresponds to a maximum wavelength cutoff of 32σ given that our simulation boxes have length 60σ. We used twice the membrane thickness, i.e., 12σ as minimum wavelength cutoff.

Model fitting. Let us explicitly write down both models being considered. According to continuum membrane theory, at zero membrane tension the fluctuation spectrum is given by [52]

$$\langle |h_n|^2 \rangle = \frac{k_{\text{B}} T}{L^2 \kappa q^4}\,, \tag{2.6}$$

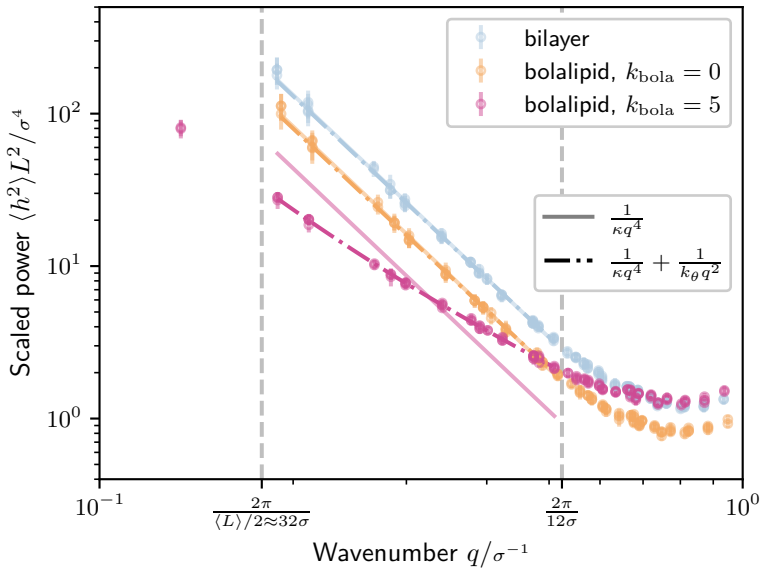

Figure 2.11: Fluctuation spectra and corresponding fits for a model without and with tilt modulus, for a bilayer membrane at $T_{\mathrm{eff}} = 1.2$, a flexible bolalipid membrane ($k_{\mathrm{bola}} = 0$) and a rigid bolalipid membrane ($k_{\mathrm{bola}} = 5\, k_{\mathrm{B}}\, T$). In vertical dashed lines we marked the interval of wavenumbers that selects the modes used for fitting. The first rigid bolalipid equilibrated mode is to the left of this interval and thus excluded from the corresponding fit.

where $q = 2\pi n/L$ is the wavenumber. For the model with tilt (Eq. (2.5)), we obtain

$$\langle |h_n|^2 \rangle = \frac{k_{\mathrm{B}} T}{L^2} \left(\frac{1}{\kappa q^4} + \frac{1}{\kappa_\theta q^2} \right) \tag{2.7}$$

We fitted the data using N measurements of mean and mean standard deviation (y_i, σ_i, x_i), with $y = \langle |u_n|^2 \rangle = \langle L \rangle^2 \langle |h_n|^2 \rangle$ and $x = q = 2\pi |n| / \langle L \rangle$ to each model $f(x_i) = y_i$. In this case, the different models $f(x)$ are given by Eqs. (2.6) and (2.7), where Eq. (2.6) can be derived from Eq. (2.7) by formally setting $\kappa_\theta = \infty$. We used the reduced R^2 value as an indicator of goodness of fit, defined as $R^2 = \sum_i ((f(x_i) - y_i)/\sigma_i)^2 / N$. Reasonable values were recognized as $R^2 \leq 1$. Typical example fits are shown in Fig. 2.11.

Validation of the tilt model. R^2 is plotted together with fit results for pure bolalipid membranes and bolalipid/bilayer mixture membranes in Fig. 2.12. In the first row we show the results of the fit of Eq. (2.6) while in the second row we used Eq. (2.7). In general, for small values of bolalipid rigidity or large bilayer fraction the fits without the tilt term were still reasonable. However, as the bolalipid rigidity increased or the bilayer fraction decreased the fits became worse. Then only fits with the tilt term were reasonable. In addition, we plot the same measures for temperature sweeps for the bilayer at $T_{\mathrm{eff}} = 1.2$, the flexible bolalipid and the rigid bolalipid membranes in Fig. 2.13. The results are summarized for all membrane types in Fig. 2.8.

We omitted the error when less than the unit. Moreover, the low values of tilt modulus will necessarily be accompanied of smaller error bars since the smaller the value, the larger the influence the term will have on the amplitudes.

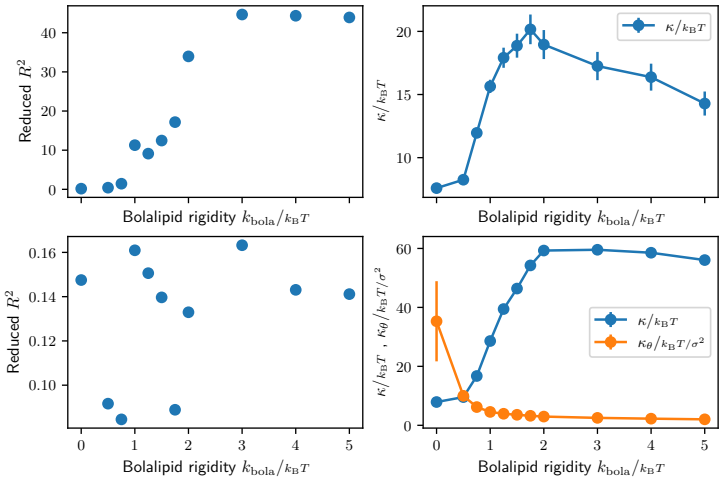

(A) Bolalipid Membranes

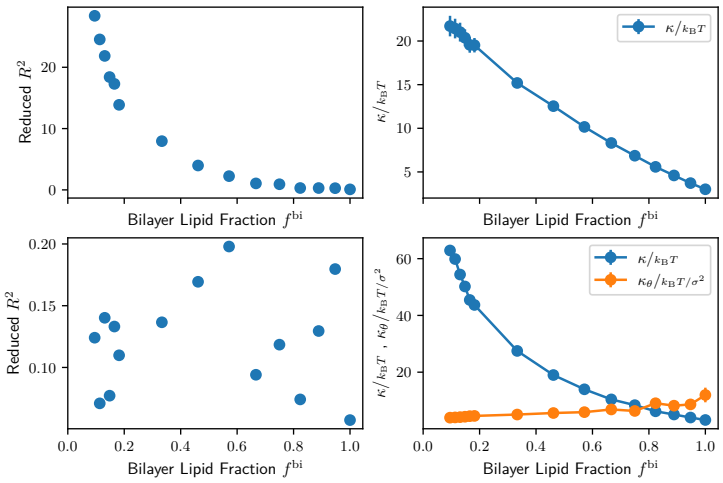

(B) Mixture Membranes

Figure 2.12: Fluctuation spectrum fit comparisons for pure bolalipid membranes (A) and bolalipid/bilayer mixture membranes (B). In the first row we show the results of the fit of the model without tilt (Eq. (2.6)) while in the second row we used the model with tilt (Eq. (2.7)).

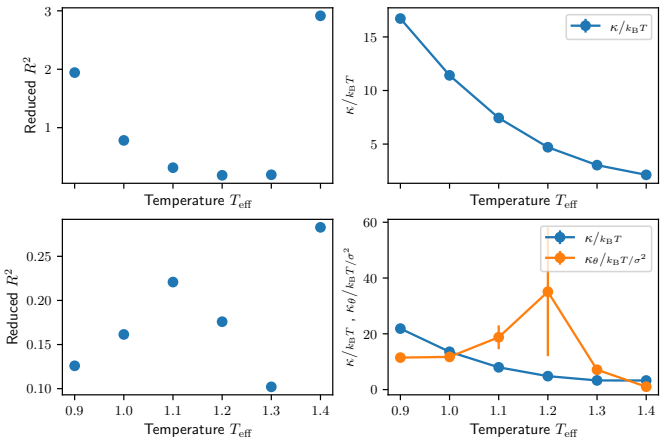

(A) Bilayer membranes fluctuation spectrum fits.

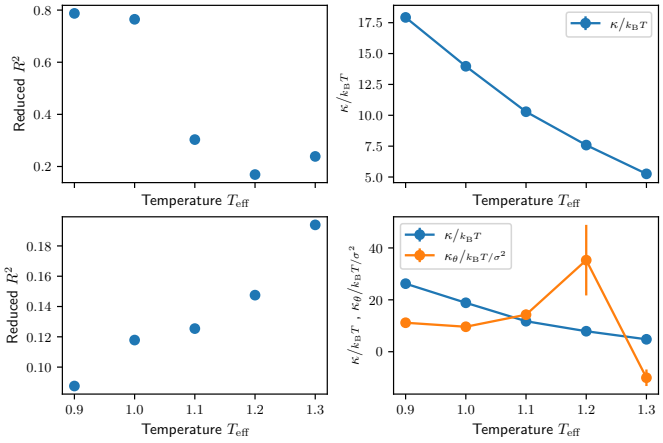

(B) Flexible bolalipid membranes fluctuation spectrum fits.

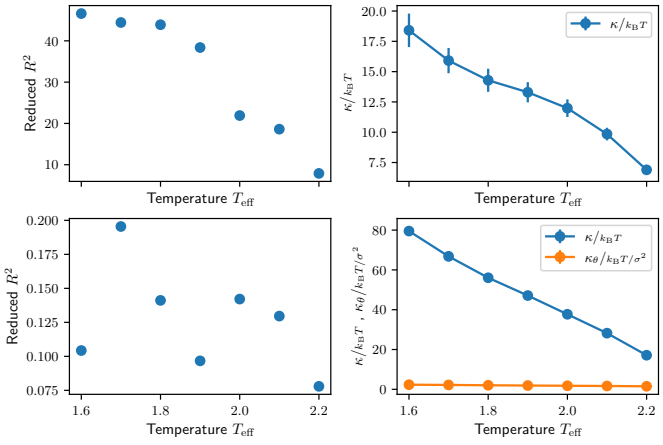

(C) Rigid bolalipid membranes fluctuation spectrum fits.

Figure 2.13: Fluctuation spectrum fit comparisons for pure bilayer membranes (A), flexible (B) and rigid pure bolalipid membranes (C), as a function of T_{eff}. For each membrane, in the first row we show the results of the fit of the model without tilt (Eq. (2.6)) while in the second row we used the model with tilt (Eq. (2.7)).

CHAPTER 3

Bolalipid membrane reshaping

To investigate the response of bolalipid membranes to large membrane curvature and topology changes like those induced upon vesicle budding, which regularly occurs in archaea, we simulated membrane wrapping of an adhesive cargo bead. Importantly, this provided us with a method to study how lipid organization is affected by externally imposed membrane curvature and mechanics. First, we cover the necessary simulation protocol in Section 3.1 and the analysis of the membrane structure in Section 3.2. Then, we go over the main results for pure bolalipid membranes in Section 3.3 and bilayer lipid / bolalipid mixtures in Section 3.4. We take a comparative look at membrane tension in wrapped cargo beads in Section 3.5, before concluding in Section 3.6.

3.1 Simulation protocol for cargo budding

To model a spherical cargo of radius $R_{\mathrm{c}} = 8\sigma$ being adsorbed by a membrane, we set up a Lennard-Jones potential between the cargo and lipid beads using Eq. (2.2). We parametrize the strength of the potential $U_m = \epsilon_{\mathrm{mc}}$, calling ϵ_{mc} the adsorption energy. With lipid tail beads, the interaction is purely repulsive, with $r_m = r_c = 2^{1/6}(8 + 0.5)\sigma \approx 9.5\sigma$. With lipid head beads, we set up an attractive well by setting $r_c = 2^{1/6}(8 + 0.5) \cdot 1.2\sigma \approx 11.5\sigma$, giving the well a width of $\approx 2\sigma$. This limits this attractive interaction to the head beads of the membrane leaflet closest to the cargo.

For budding simulations, we first pre-equilibrated for $10^4\tau$ a membrane with 60^2 head beads per leaflet before placing the cargo bead on top of the membrane. To displace any lipids that might be inside the cargo's volume, we performed a short run in the constant volume ensemble, while scaling from zero to full strength the membrane-cargo interaction. We then ran the simulation at constant pressure until the system was in equilibrium for at least $\Delta_{\mathrm{eq}} = 30 \times 10^3\tau$; the end state should then be either partial or full membrane budding. In practice total runtime was $\Delta_{\mathrm{total}} \in [60, 120] \times 10^3\tau$. For a significant region of membrane parameters of interest, as we increased ϵ_{mc} we observed the equilibrium state transition directly from non-budded to a collapsed state with the membrane folded around the cargo in a small simulation box. To impose the existence of a region with budding we kept all membranes in budding simulations minimally stretched by setting the barostat target lateral pressure to $P_{\mathrm{xx}} = P_{\mathrm{yy}} = -0.001 k_{\mathrm{B}} T/\sigma^3$.

Note that it was not possible to measure ϵ^*_{mc} for pure bilayer membranes at chosen parameters for mixtures (same as in Section 2.4) since budding was always followed by membrane disassembly as the bilayer membrane is close to the gas phase for the used parameters.

3.2 Analysis of membrane structure and lipid conformation

We developed a pipeline for analysing each frame of membrane simulation trajectories, using the pipeline framework and components from OVITO [56].

Cluster identification and surface reconstruction. We distinguished and identified clusters by fitting mean position and orientation of lipids to the expected membranes: a horizontal plane for the flat membrane simulations and the mother membrane in budding simulations and a sphere for the budded membrane in budding simulations. We constructed the membrane surface from the set of lipid beads using the alpha-shape method with radius 1.5σ (implemented in [56]); this ensures any pore of diameter $> 1\sigma$ will be not be closed over by the resulting surface.

Midplane construction. We then constructed the midplane of the membrane by clustering the faces of the Voronoi diagram of the membrane surface vertices that are nearly coplanar and inside the membrane surface and then meshing the resulting oriented point cloud. This procedure is general enough to work for pre-budding frames of the budding simulations. The midplane orientation is adjusted to be consistent frame to frame.

Membrane pore identification. By computing the signed distance to the midplane, we assigned a leaflet to each membrane surface element. We then intersected the membrane surface with the midplane surface, obtaining for each pore a line marking its perimeter. For our purposes it was sufficient to project each pore perimeter into a least-squares fitted plane and compute the area and perimeter from the projected line. To perform leaflet area measurements we considered the two surfaces at equal distance between the membrane surface and the midplane. For the measurements of pore diameter in Fig. 3.1D and Fig. 3.4D, we first took the ensemble average, i.e. time average with rescaling of std. mean deviation according to autocorrelation, of the total pore area.

We only consider a point to be part of a pore if its projection in the midplane membrane is within 3σ of its surface. To each point we assign a leaflet corresponding to its signed distance to the midplane. We apply this location classification to the head bead of each bilayer lipid and each half of a bolalipid. Due to the bolalipid's symmetry, some combinations of conformation (given by the sign of the angle between their head beads) and location are indistinguishable, while others are transition ephemeral states that for our ensemble measures were not relevant (e.g., U-shapes that have one head bead in each layer). When both head beads are on the same leaflet, the only relevant states are the U-shape, where the heads beads angle is $\leq \pi/2$ and the flat state, where the angle is $> \pi/2$. When the head beads are in different leaflets, we get the straight state. Thus, each lipid is assigned a state, some of which have a leaflet; additionally we consider a lipid to be in a pore if any of it(s) head bead(s) is near a pore.

Lipid specie/conformation per leaflet. For analysing membrane composition in lipid specie and conformation, we compute and present specie/conformation fractions in each leaflet,

not as fraction of total number of lipids, but as amount of head fractions over total number of head beads in a leaflet. In this way, the denominator is a function of geometry and thus approximately conserved. For instance, the fraction of head beads that belong to bilayer lipids $f_{\mathrm{h}}^{\mathrm{bi}}$ is related in the following way to the fraction of lipids that are bilayer lipids, f^{bi}

$$f_{\mathrm{h}}^{\mathrm{bi}} = \frac{n^{\mathrm{bi}}}{n^{\mathrm{bi}} + 2n^{\mathrm{bola}}} = \frac{1}{\frac{2}{f^{\mathrm{bi}}} - 1} \tag{3.1}$$

For instance, for $f_{\mathrm{h}}^{\mathrm{bi}} = 10\%$ of the head beads to belong to bilayer lipids, we need the bilayer lipid fraction to be $f^{\mathrm{bi}} \approx 18\%$.

Quantifying lipid distribution mid-budding. To capture the membrane structure mid-process of budding, we take advantage of the near axially symmetric profile around the cargo bud. To do this, we chose a trajectory section that is short enough so that the shape of the membrane is roughly static. In practice, this corresponded to a 2000τ time interval, where we then sample uniformly 100 frames. For each frame, we take a cylindrical section of the simulation centred on the membrane and axis pointing upwards towards z. We compute for each lipid the property of interest(bolalipid conformation for pure bolalipid membranes or lipid species for mixture membranes) and assign it to each of its constituent particles. Using the cargo bead as the origin for cylindrical coordinates (r, θ, z), dropping the angle, and using hexagonal binning on the r, z plane, for each bin we compute both the average value of the quantity of interest and the total number of particles observed. Using these totals we then threshold on a minimum number of 40 particles observed per bin and plot the composition as a fraction of $(\#\text{studied conformation or specie}) \,/\, (\text{total in bin})$.

3.3 Curving bolalipid membranes

We first simulated membrane wrapping at different adsorption energies ϵ_{mc} between lipid head beads and the cargo until we observed that the membrane wrapped the cargo completely (including membrane fission). Then the minimum adsorption energy, for which a membrane bud completely enveloped the cargo bead, is the onset adsorption energy $\epsilon_{\mathrm{mc}}^{*}$ (Fig. 3.1A), which we measure as a function of the bolalipid stiffness k_{bola} (Fig. 3.1B). For small molecular stiffness k_{bola}, $\epsilon_{\mathrm{mc}}^{*}$ first increases linearly with k_{bola} before it saturates around $k_{\mathrm{bola}} = 3\, k_{\mathrm{B}}\, T$. We expect that the onset energy is proportional to the membrane bending rigidity $\epsilon_{\mathrm{mc}}^{*} \propto \kappa$, because the bending energy to wrap a spherical particle is size-invariant [18, 19]. When we increased the bending rigidity, through increasing stiffness of bolalipid molecule k_{bola}, $\epsilon_{\mathrm{mc}}^{*}$ increased by a factor of 3 (Fig. 3.1B), suggesting that also κ increased by a factor of 3. However, from directly measuring the membrane rigidity from the fluctuation spectrum (Fig. 2.4C), we saw that κ increased by a factor of 10. To reconcile these seemingly conflicting observations we reason that the bending rigidity κ, similar to Fig. 4.1C, is not constant but softens upon increasing membrane curvature, due to dynamic change in the ratio between bolalipids in straight and U-shaped conformation. Hence, bolalipid membranes show stroking plastic behaviour as they soften during reshaping.

Through analysing the bolalipid conformations (as described in Section 3.2), we found that the membrane was able to curve by increasing the fraction of U-shaped bolalipids in the outer layer of the deformation. We observed this qualitatively during the budding process (Fig. 3.3), where this effect is also slightly visible on the inner membrane neck, and exhaustively quantified it after budding (Fig. 3.1C). Remarkably, though, even when lipids are so stiff that there are no

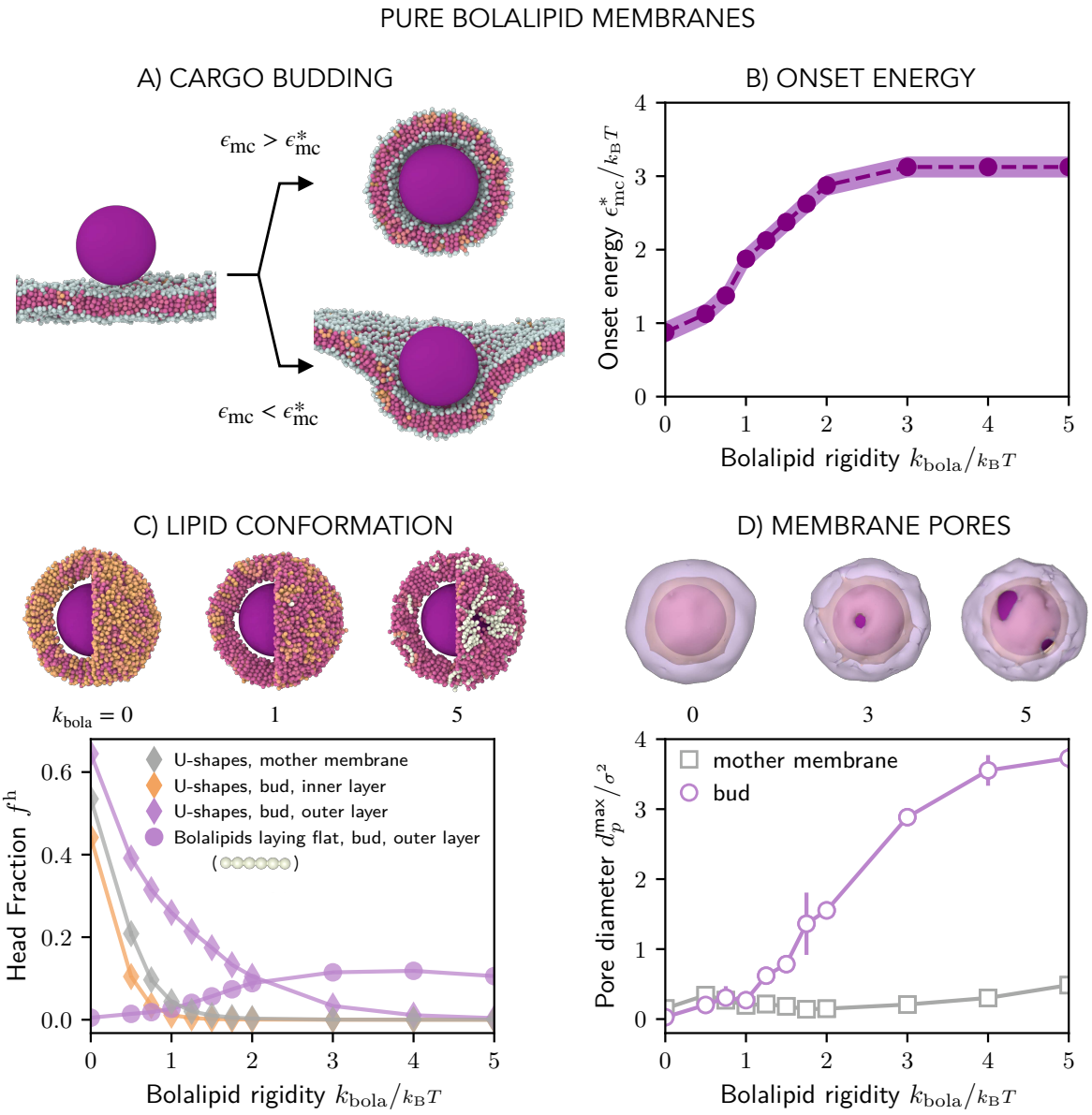

Figure 3.1: **Reshaping of pure bolalipid membranes.** (A) Simulation snapshots of the membrane wrapping a cargo bead adsorbing onto it. Above the onset adsorption energy ϵ^*_{mc}, the cargo is fully wrapped by the membrane and buds off the mother membrane. (B) Onset energy ϵ^*_{mc} as function of the bolalipid molecule rigidity k_{bola} (for the parameters defined by the line in Fig. 2.4A). (C) Bottom: Fraction of bolalipids in the U-shape conformation u_f in the outer and inner layers of the membrane bud, and in the flat mother membrane, as function of the bolalipid molecule rigidity k_{bola}. Top: Snapshots and cross-sections of the membrane around the cargo bud. At high bolalipid rigidity the pores form around the cargo, and are lined with bolalipid molecules lying flat around the pore in a straight conformation, with both heads in the outer layer (coloured in white). The rest of bolalipids coloured according to their head-to-head angle as before. (D) Bottom: Average diameter of transient pores in the membrane bud and the mother membrane as function of the bolalipid molecule rigidity k_{bola}. Pores are defined as membrane openings through which a sphere of diameter $1\,\sigma$ can cross. Top: Snapshots of the membrane surface with outer and inner leaflet surface coloured in purple and orange, respectively, intersecting at the rim of the pore (grey).

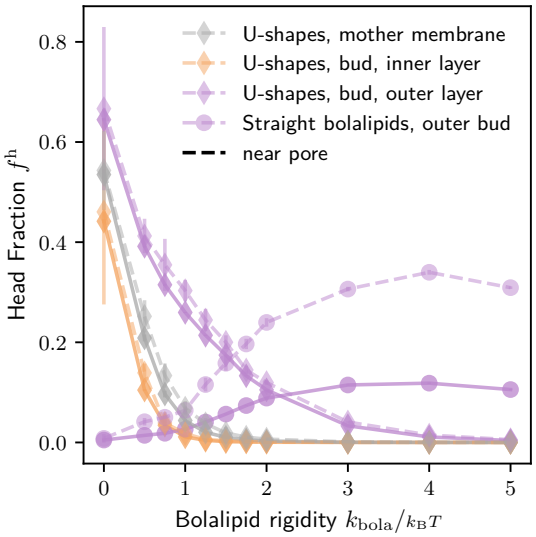

Figure 3.2: Lipid conformation and location in the membrane bud for pure bolalipid membranes, excluding lipids near pores (solid lines) and exclusively considering lipids near pores (dashed lines).

more U-shaped bolalipids in the flat mother membrane ($k_{\mathrm{bola}} = 2\,k_{\mathrm{B}}\,T$), the outer layer of the curved membrane retained a non-negligible fraction of $\approx 10\%$ U-shaped bolalipids, which in turn decreases κ and softens the membrane. However, the softening effect on the membrane, indicated through a constant onset energy for $k_{\mathrm{bola}} \geq 3\,k_{\mathrm{B}}\,T$ (Fig. 3.1B), persists even for those very stiff bolalipids. Since for stiff membranes, practically all U-shaped bolalipids are gone (Fig. 3.1C), this suggested that an additional membrane-curving mechanism must be involved.

Looking more closely, at high molecular rigidity ($k_{\mathrm{bola}} \geq 2k_{\mathrm{B}}\,T$) we observed the formation of multiple pores on the membrane bud, which we quantified by measuring the time-averaged maximum pore diameter (Fig. 3.1D, see Section 3.2 and Movie 6). While large pores were not observed in the flat membrane, the diameter of membrane pores around the cargo was found to grow with the increase in bolalipid stiffness. We reasoned that pores form when the energetic cost required to change the bolalipid conformation to release bending stress is larger than the energetic cost of opening a lipid edge surrounding the pore. Hence, for relatively flexible bolalipids, U-shaped bolalipids provide the necessary area difference between the outer and inner layer of the membrane bud and thereby soften the membrane. For stiff bolalipid molecules, however, membrane pores start to form to enable membrane curvature as U-shaped bolalipids become prohibited. Both mechanisms help to explain the discrepancy between ϵ^*_{mc} and the bending modulus κ obtained by studying membrane fluctuations (Fig. 2.4C).

3.3.1 Pore effect on lipid conformation

For simulations where pore formation was significant, namely the simulations with pure bolalipid membranes, we presented before (Fig. 3.1C) conformation measurements that exclude lipids that are in a pore. To investigate the effect of the pores on lipid conformation, we redid these measurements, considering exclusively lipids near pores and compared with those that only include lipid $3\,\sigma$ away from pores (see Fig. 3.2). Not surprisingly, the only value to change significantly is the fraction of flat bolalipids, which is much larger near pores.

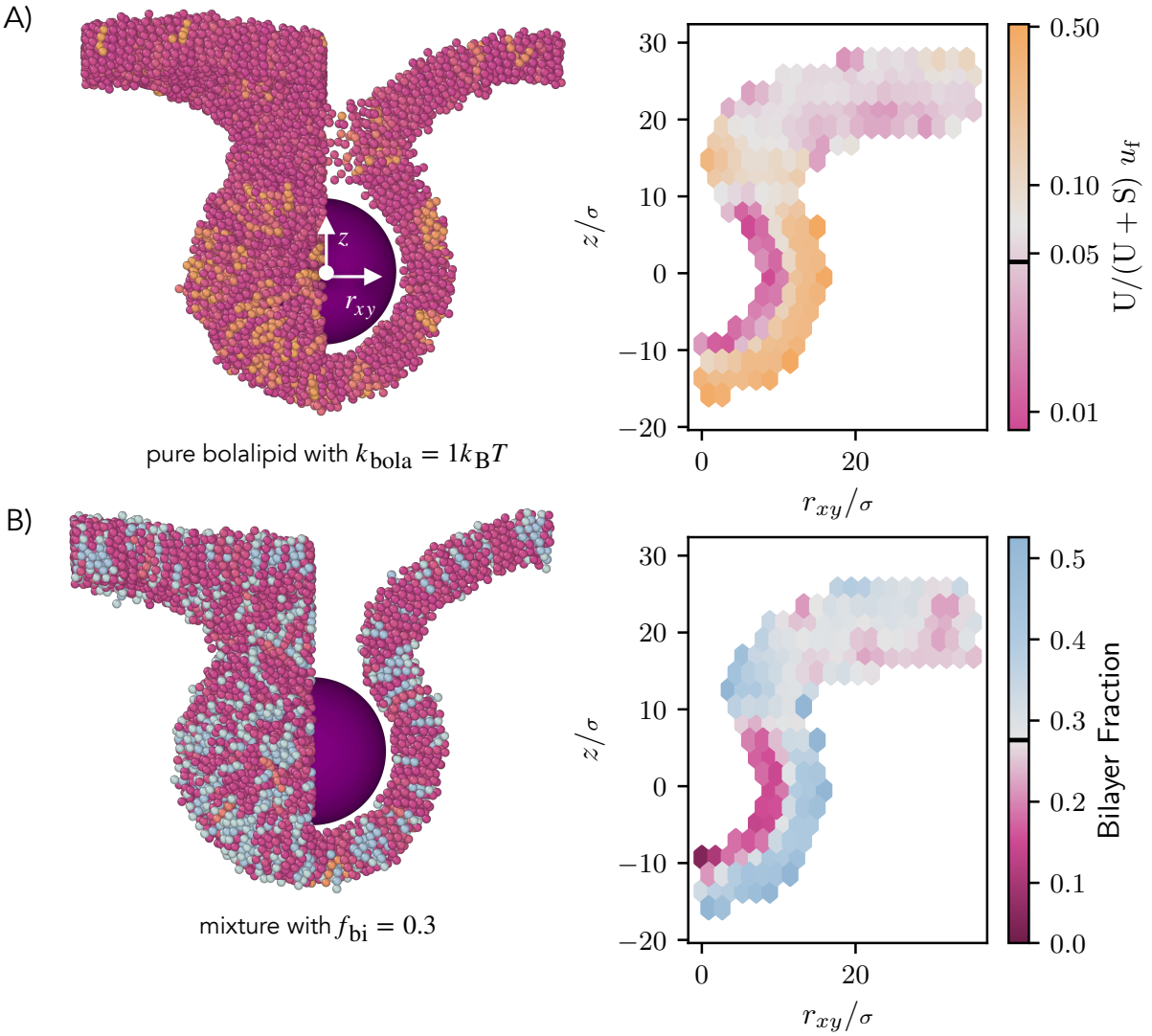

Figure 3.3: Lipid conformation and location in the membrane bud for pure bolalipid membranes, before budding, (A) for pure bolalipids at $k_{\mathrm{bola}} = 1\,k_{\mathrm{B}}\,T$ and for (B) a mixture of bolalipids with 30% bilayer, method described in Section 3.2. For both cases, a snapshot (left) is shown with the front right half of the membrane cut away, showing the profile shape, matching the (right) time averaged spatially varying conformation or specie fraction. Visible at $z > 10\,\sigma$ and for small r_{xy} is the inner region of the neck. While for mixture membranes the effect on bilayer fraction is visible using a linear scale, for bolalipid membranes at $k_{\mathrm{bola}} = 1\,k_{\mathrm{B}}\,T$ the effect spans multiple orders of magnitude, so a logarithmic scale was used. The flat membrane values, taken as average values of the bins at $r_{\mathrm{xy}} > 20\,\sigma$, are indicated by a black mark on the colour bar.

3.4 Curving archaeal membranes

Having shown that bolalipid membranes can effectively soften also by including some amount of bilayer-forming lipid molecules, we next measured the onset energy $\epsilon^*_{\rm mc}$ for cargo budding in the membranes formed by mixtures of bolalipids and bilayer-forming lipids, as a function of bilayer lipid head fraction $f_{\rm h}^{\rm bi}$ (Fig. 3.4A and Movie 5.d). We found that the onset energy sharply decreases with increasing amount of bilayer forming lipids, and plateaus for 50% bilayer head fraction, where it acquires similar values as in the case of fully-flexible bolalipids (Fig. 3.1B). For small bilayer fractions, U-shaped bolalipids localize almost exclusively on the outer layer of the bud (Fig. 3.4B). As the bilayer fraction increases, there is a steady reduction in the percentage of U-shaped bolalipids in the outer layer in favour of bilayer lipids that take their role in supporting membrane curvature, with U-shaped bolalipids completely vanishing at high fractions of bilayer-forming lipids. A fraction of bilayer lipid head beads initially shows an asymmetry between the preferred outer layer and the penalized inner layer around the cargo (Fig. 3.4C), but eventually approaches $f_{\rm h}^{\rm bi}$ in both layers. Taken together, as the bilayer lipid fraction increases, the role of U-shaped bolalipids in making up the asymmetry between the outer and inner layer, is taken over by bilayer lipids. Curiously, the addition of bilayer lipids promotes the formation of U-shaped lipids, both in the flat membrane and even in the inner layer around the bud. This is likely to be explained by the fact that when more bilayer lipids are incorporated, the membrane is less densely packed (Fig. 3.5B) and thus U-shaped bolalipids are promoted.

Importantly, we observed nearly no pores in the membrane bud in mixed membranes, even when we only had very little fraction of bilayer-forming lipids (Fig. 3.4D). Only as the bilayer fraction increased, we observed the formation of very small pores in the bud. For the flat mother membrane, however, membrane pores started to form with increasing values of $f_{\rm h}^{\rm bi}$. They acquired sizes similar to those obtained around the bud in pure bolalipid membranes (Fig. 3.1D). The pore formation in the flat mother membrane is likely promoted because the membrane becomes destabilized by the increasing proportion of bilayer lipids which are close to the gas phase. Taken together, bolalipids can bud porelessly when bilayer-forming lipids, which cause membrane softening, are included.

3.5 Membrane tension in bud

In our budded membranes, the area in each layer is different. By starting from a flat membrane that is then wrapped around the bud, our setup forces the membrane to either tension each layer differently, in the extreme forming pores, or to move particles from the inner to the outer layer. Since we have extensively documented the former two phenomena, we now take a look at tension in each leaflet of the bud. We can use the area per head as a proxy for tension, by comparing with the values for the flat mother membrane. We note that these measurements excluded membrane within $3\,\sigma$ of a pore. When tension is positive, the membrane will be stretched, and thus the area per head will be above that of the mother membrane. If tension is negative, the membrane will be compressed, and thus the area per head will be below that of the mother membrane. We plot our measurements in Fig. 3.5A, which shows the area per head bead as a function of $k_{\rm bola}$ in the inner and outer layer of the membrane bud, with the flat mother membrane for comparison.

We can fully interpret the trends shown. The plot shows that for bolalipid membranes the area per head is non-monotonic in $k_{\rm bola}$. For flat bolalipid membranes (mother membrane, grey

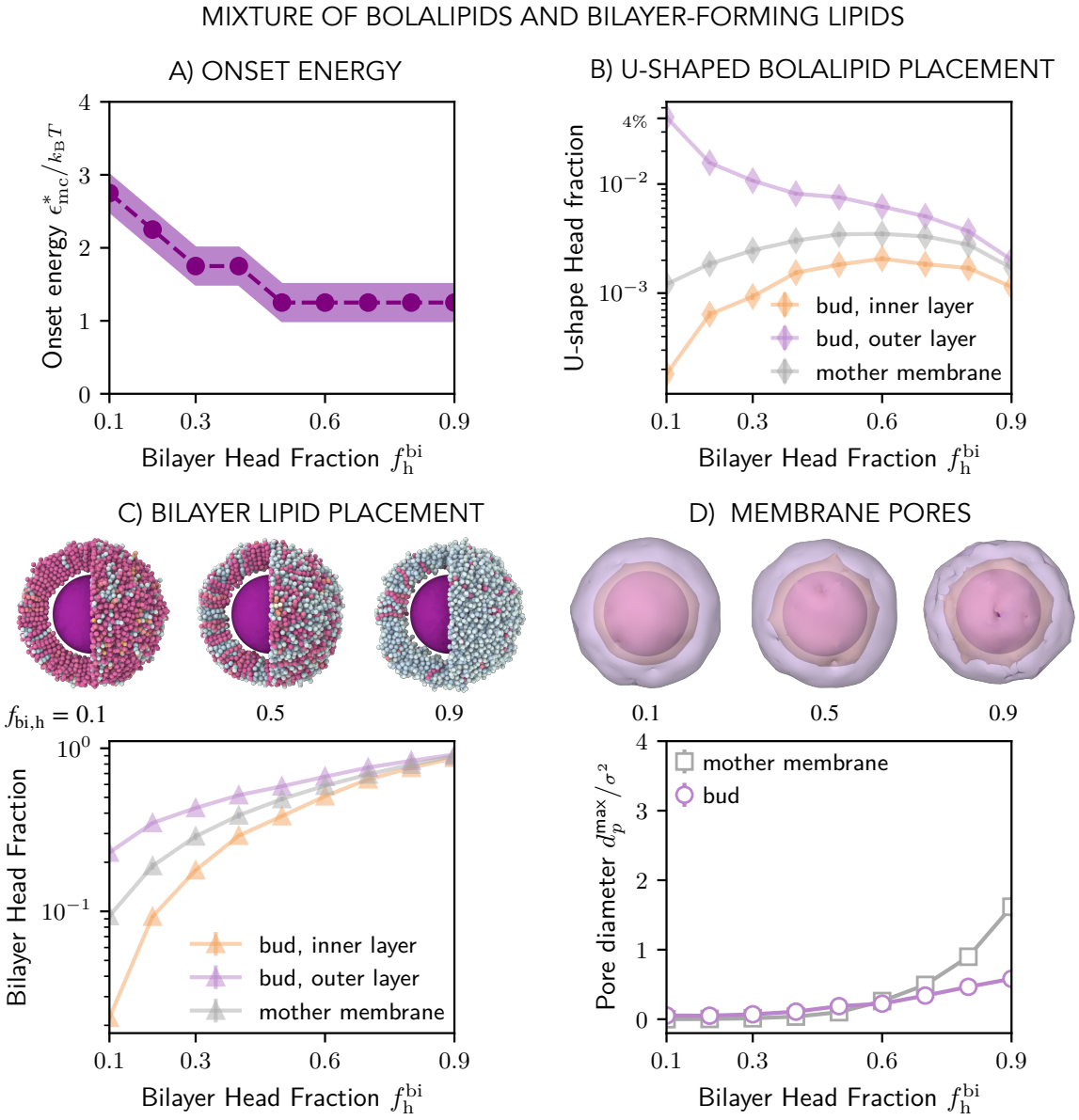

Figure 3.4: **Curving of the mixed membranes, made of bilayer and bolalipid molecules.** (A) Onset energy required to form the membrane bud, $\epsilon^*_{\rm mc}$, as function of bilayer head fraction $f_{\rm h}^{\rm bi}$ (for the parameters defined in Fig. 2.9.) (B and C) Fraction of U-shaped bolalipid (B) and bilayer (C) head beads in the outer and inner layers of the membrane bud and in the flat mother membrane as a function of the bilayer head fraction $f_{\rm h}^{\rm bi}$. Top panels show the respective snapshots of membrane surface around cargo, where bilayer lipids are shown in light blue as in Fig. 3.1. (D) Average diameter of transient pores in the membrane bud and the mother membrane as function of bilayer head fraction $f_{\rm h}^{\rm bi}$ and respective snapshots of membrane leaflet surfaces surrounding the bud (Top panel).

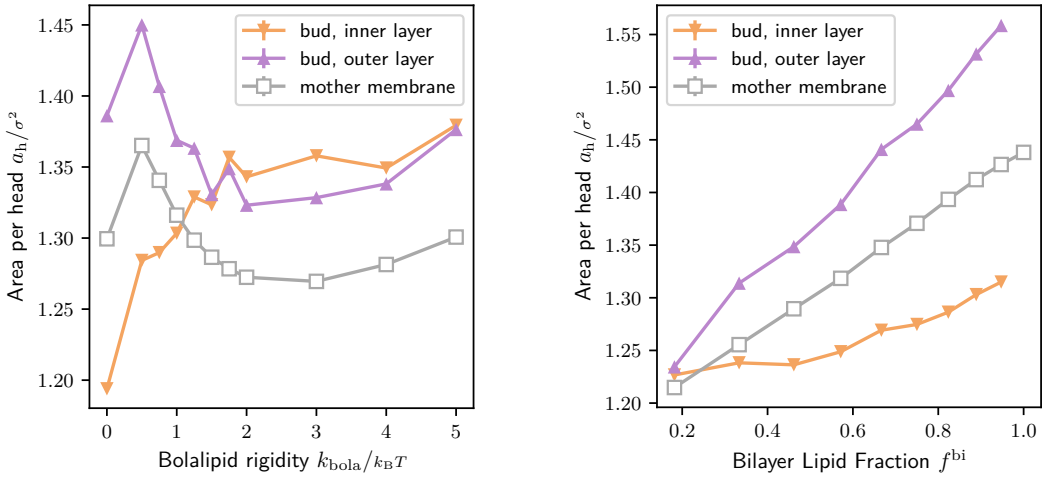

(A) Bolalipid membranes. (B) Mixture membranes.

Figure 3.5: (A) Area per head bead as a function of k_{bola} in the inner and outer layer of the membrane bud and the flat mother membrane. (B) Area per head bead as a function of the bilayer lipid fraction f^{bi}; for this plot we used the bilayer lipid fraction instead of the bilayer head fraction to evidence the linear trend for the mother membrane (grey).

line), the trend inversion for bolalipids at $k_{\mathrm{bola}} = 0.5\, k_{\mathrm{B}}\, T$ can be understood by considering our choice of T_{eff} for each k_{bola} changes slope at the same point (see Fig. 2.4A); after this sudden change, the area per head quickly decreases by 10%, stabilizing at the same $k_{\mathrm{bola}} = 2\, k_{\mathrm{B}}\, T$ value where U-shapes vanish completely, before slowly increasing by 4% as k_{bola} reaches the end of the range. In contrast, for membrane mixture of bilayer and bolalipids the area per head as a function of the bilayer lipid fraction f^{bi} monotonically increases (Fig. 3.5B), varying by $\approx 10\%$. By default, both inner and outer leaflet would be relaxed if possible, at the same value of area per head as the flat mother membrane. However, the cargo bead competes with tension and pulls head beads from the outer to the inner layer, thus increasing the area per head for the outer layer and decreasing it for the inner layer. This happens both for relatively flexible bolalipids and mixture membranes with increasing bilayer fraction, which can indeed move head beads between leaflets, by, respectively, forming and/or flip-flopping U-shaped bolalipids, and flip-flopping bilayer lipids. When this is not possible, the area per head values for inner and outer layer are roughly equal, such as for the mixture membranes with nearly no bilayer lipids at $f^{\mathrm{bi}} = 0.1$. This also happens for bolalipids with $k_{\mathrm{bola}} > 2\, k_{\mathrm{B}}\, T$, where we note that the area per head for the bud layers are higher than that for the relaxed membrane; this can be understood by considering that at these k_{bola} values the bud membrane has pores, whose line tension then competes with tension, stretching the membrane.

3.6 Discussion

To investigate how bolalipid membranes respond to changing membrane curvature, we performed simulations in which small cargo particles budded from flat membranes. We found that by enforcing curvature on bolalipid membranes, the fraction of U-shaped bolalipids increased around the cargo bud, especially in the outer membrane layer and hence softened the membrane. As another mechanism to release curvature stress we observed the formation of membrane pores, which could be mended by adding small amounts of bilayer lipids, similar to the mixture membranes that are found in archaea [60]. Our results suggest that enforcing membrane

bending can soften bolalipid membranes locally by increasing the number of U-shapes, rendering the membrane a mechanically switchable material where large curvature decreases stiffness.

Taken together, our results show how membranes which are mixtures of bilayer and bolalipids maintain cell integrity at high temperatures, while also undergoing leak free membrane bending. This suggests that archaeal membranes can balance opposing needs when adapting to extreme environmental conditions.

CHAPTER 4

Bolalipid membrane plasticity

In this chapter, we investigate how bolalipid membranes respond to mechanical deformations. While in Chapter 2 we concerned ourselves with properties at near zero curvature and tension, here in Section 4.1 we show that the promotion of U-shapes upon deformation makes the bending modulus of bolalipid membranes curvature dependent. In section Section 4.2, we inspect a regime that remains problematic to probe, that between low and high curvature, and make steps towards a novel measuring method. In Section 4.3, we show that membrane tension is also coupled to lipid conformation. Finally, in Section 4.4, we reflect on these findings.

4.1 Interplay between membrane curvature and rigidity

Following geometric intuition, we expect the fraction of molecules in the U-shape to change as the membrane curvature changes, to enable area difference between the two membrane leaflets needed to adapt to the curvature. Since forming U-shapes for $k_{\mathrm{bola}} > 0$ requires spending energy, this would imply that the bending rigidity, importantly, through the fraction of U-shaped bolalipids, is curvature dependent. We will now take a theoretical detour to develop this idea.

Consider a membrane patch of area A, thickness h and mean curvature $H = \frac{C_1+C_2}{2}$, set up so that no flow of lipids is allowed in or out. Make its lipids components be mostly straight bolalipids. The flow restriction could happen either due to a geometrical constant, e.g. a closed vesicle, or, for instance, by a separation of timescales, where bending is much faster than the flow of bilayer lipid components. In a membrane of mostly straight bolalipids, the bilayer components are the few U-shapes, whose flow is hampered by the transmembrane, monolayer components (straight shapes).

Let us further impose that the area difference energy dominates, an assumption we will come back to later. For a spherical membrane of radius R, the area difference is:

$$\Delta A = A\left(\frac{R+h/2}{R}\right)^2 - A\left(\frac{R-h/2}{R}\right)^2 = A2h/R = A2hH$$

, so linear in mean curvature. For a cylindrical membrane of radius R, the area difference is

$$\Delta A = A\left(\frac{R+h/2}{R}\right) - A\left(\frac{R-h/2}{R}\right) = Ah/R = A2hH$$

, i.e. exactly the same. For the general case, the area element at height z above the membrane midplane, on the arc lengths $s_1\, s_2$ is $dA(z) = (1 + zC_1)(1 + zC_2)\, ds_1\, ds_2$. Therefore, the area difference is:

$$dA(h/2) - dA(-h/2) = h(C_1 + C_2)\, ds_1\, ds_2 = 2hH dA$$

This general approach can fail for large deformations where the expansion is incorrect in that h is of the same order as $1/H$, but for the special cases of a sphere or a cylinder, the first approach works regardless.

Let us assume that in this system the area difference can only be compensated by the change of conformation of the U-shapes, and not by the extension/compression of the outer/inner leaflets of the membrane. The conformation change has fixed cost E_u per bolalipid. So the energy change from flat to curved becomes $\Delta E_{\Delta A} = \frac{E_u}{A_u} A 2h|H|$, where ρ_u is the area per U-shape. This linear dependency on the modulus of the curvature is unlike a mix of a mean and gaussian curvature term, since it does not have a square term on C_i. From a theoretical perspective, having an energy with a term that is discontinuous in its first derivative can lead to bistability, hysteresis, energy barriers, metastability. Contrast with a x^2 term, where the force $-x$ scales down, proportionally with the coordinate as the origin is approached. It is known that pure bilayer membranes follow x^2 behaviour up to extreme curvatures [28]. Consequently, in the limit of small x, bolalipid membranes should then respond faster than pure bilayer membranes.

We now come back to the assumption that the area difference energy dominates the membrane energy. We will hold the assumption that area difference energy forces the number of U-shapes, however we will now argue that the intra-leaflet bending energy term is negligible. In our model, coexisting bilayer lipids and bolalipids with the same parameters was only possible by placing bilayer lipids in their phase diagram close to their gas region, which simultaneously placed bolalipids near their respective gel region. One can then interpret the low bending modulus of the pure bilayer lipid membranes near their gas region as the bending modulus corresponding to the intra-leaflet bending energy of a pure bolalipid membrane near their gel region; as we would move up in the phase diagram with our pure bolalipid membrane, we would expect this intra-leaflet bending modulus to decrease. This supports considering this intra-leaflet bending modulus κ_i as smaller than $10\, k_\mathrm{B} T$.

The energy of the pure bolalipid membrane patch then can be written $\Delta E = \Delta E_{\Delta A} + \Delta E_\mathrm{b}$, where $\Delta E_\mathrm{b} = 2\kappa_\mathrm{i} H^2 A$. We can then compare the terms:

$$\begin{aligned} \frac{\Delta E_{\Delta A}}{\Delta E_\mathrm{b}} &= \frac{\frac{E_u}{A_u} A 2h|H|}{2\kappa_\mathrm{i} H^2 A} \\ &= \frac{E_u}{A_u} \frac{h}{\kappa_\mathrm{i}|H|} \end{aligned} \tag{4.1}$$

Plugging in values from our model at $k_\mathrm{bola} = 1k_\mathrm{B}T$, $E_u = 2k_\mathrm{bola} = 2k_\mathrm{B}T$, $\kappa_\mathrm{i} \leq 10k_\mathrm{B}T$, $h = 4\sigma$, $A_u \approxeq 2 \cdot 1.2\sigma$, we get that the area difference term dominates if $1/|C| \gg 1$, i.e. for radius of curvature $\gg \sigma$; this applies to our budding and bending simulations.

Of course, these two terms are not the full picture when it comes to the Hamiltonian of a bolalipid membrane. Most importantly the membrane can adjust the tension in each leaflet separately, forgoing forming U-shapes, and instead compressing or stretching. To investigate this, we measured the bending rigidity, or more correctly, the resistance to bending, of bolalipid membranes in cylindrical shapes as a function of their radii.

4.1.1 Simulation setup and analysis

We generally follow the method described by Harmandaris in [28]. In their paper, the force F_x exerted by a cylindrical membrane of radius R on a fixed dimensions simulation box along the cylinder axis ($\hat{x}$) is related to the bending modulus by $F_x R = 2\pi\kappa$. We can write $F_x = 2\pi R\Sigma$, where Σ is the membrane tension, and we recover the equation used to fit membrane tethers, $R = \sqrt{\frac{\Sigma}{\kappa}}$. In our case, it is more helpful to consider F_x as the force that opposes the system expansion and thus $F_x = \frac{d\mathscr{F}}{dL_x}$, where $\mathscr{F}$ is the free energy of the system, function of L_x, the cylinder length. L_x is also the simulation domain x axis length, so we can compute F_x by taking the ensemble average $\langle\sigma_x L_y L_z\rangle$, where σ_x is the xx component of the system stress tensor.

To consider a curvature dependent bending modulus $\kappa(H)$, we must first replace the typical bending energy per area term $2\kappa H^2$ in the membrane Hamiltonian by a term $\epsilon(H)$ dependent on the mean curvature H. In this case, under the assumption of constant membrane area, one gets:

$$\frac{FR}{2\pi} = \frac{1}{4H}\frac{d\epsilon}{dH} = \kappa(H) \tag{4.2}$$

For all measurements we ran 4 seeds, each over $20 \times 10^3\,\tau$, integrating in the NVT ensemble using a Langevin thermostat with damping coefficient 1τ and unit temperature. The membrane was assembled into a cylindrical shape, with the number of heads in each leaflet pre-balanced. The stress tensor was measured at 1τ intervals. The radius was measured from trajectory frames saved every 20τ in the following way. First we excluded lipids in gas phase by clustering. Then we computed the centre of mass of the membrane and set it as our origin for the cylinder cross-section x-y plane. Then we computed the measured radius as $R = 1/\langle 1/r\rangle$, where the average is over beads and where $r = |x^2 + y^2|$ is the distance to the cylinder axial radius. Using $1/r$ instead of r directly compensates to first order for the shell volume $2\pi r dr$ dependency on r.

After qualitatively checking for quick equilibration of the radius, fraction of U-shaped conformers and the stress tensor components, we dispensed with lengthy equilibration, discarding only the first 1000τ of the trajectory. These observables were then averaged over rest of the trajectory, with errors determined in a blocking-equivalent manner. The proponents of the method noted that for their coarse-grained membranes, it was necessary to reduce the timestep from the usual 0.01τ used in previous work [17] by a half or a tenth, to $0.005 - 0.001\tau$. This was so that the transversal components of the stress were near-zero, as expected since the system does not cross the x or y boundaries. Therefore, to guarantee correct integration, we lowered the timestep until the ratio $|(P_x + P_y)/(2P_z)|$ was less than 0.1. We also balanced increasing the cylinder length, to improve statistics on the stress tensor measurement, against computational performance and the occurrence of long-term deviations from cylindrical shape at high aspect ratio R/l_z. This agrees with the claims by the authors of [28] that in first approximation the first modes of fluctuation along the cylinder axis counteract the ones along the cylinder cross-section. To the best of our knowledge, however, the related theoretical justification cited in the same paper was never published.

Since the simulation of cylinders implies a careful choice of parameters to guarantee a valid measurement of the bending modulus, we include the exact parameters and results in Tables 4.1 to 4.3.

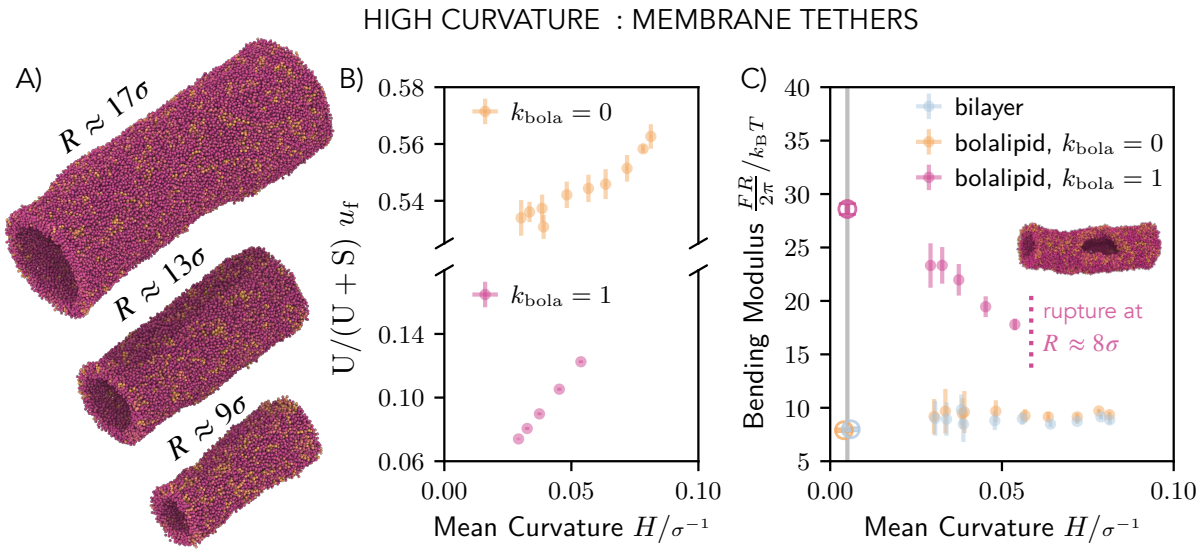

Figure 4.1: **Mechanics of pure bolalipid membranes at high curvature.** (A) Snapshots of bolalipid membranes at the range of explored curvatures for $k_{\mathrm{bola}} = 1k_{\mathrm{B}}T$. (B) Fraction of bolalipid molecules in the U-shaped conformation as a function of the mean membrane curvature $H = 1/(2R)$ for membranes made of flexible ($k_{\mathrm{bola}} = 0$) and semi-flexible ($k_{\mathrm{bola}} = 1k_{\mathrm{B}}T$) bolalipid molecules. (C) Bending modulus as a function of curvature. For the flat membrane ($H \sim 0$), the corresponding bending rigidity from (C) is marked by the vertical line and empty circles.

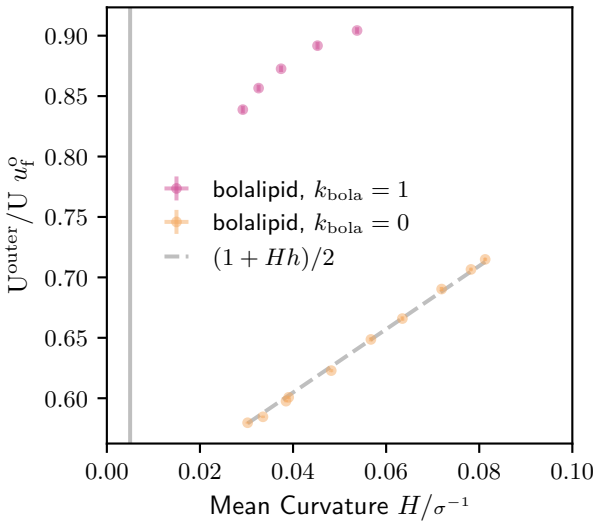

Figure 4.2: Fraction of U-shaped bolalipids in the outer layer of membrane cylinders of bolalipids at $k_{\mathrm{bola}} = 0$ and $k_{\mathrm{bola}} = 1\,k_{\mathrm{B}}T$, as a function of different curvatures H. For flexible bolalipids ($k_{\mathrm{bola}} = 0$) we show the best fit to the equal distribution hypothesis corresponding to the membrane thickness $h = 5.23 \pm 0.01\sigma$.

4.1.2 Results

We first noticed that while membrane tubes made of bilayer and flexible bolalipids were stable up to small cylinder radii R, almost as small as the membrane thickness itself, we found that membrane made from stiffer bolalipids ($k_{\mathrm{bola}} = 1 k_{\mathrm{B}} T$) ruptured well before (Fig. 4.1C, snapshot). We found this rupture was preceded by a membrane softening: for these stiff bolalipids, as the membrane mean curvature increases the bending rigidity κ decreases linearly by up to 40% (Fig. 4.1C). In contrast, we did not find that κ was curvature-dependent for bilayer or flexible bolalipid membranes ($k_{\mathrm{bola}} = 0$).

We can further examine this difference by comparing hamiltonians. Naming $H_{\mathrm{max}} \approx 0.06\sigma^{-}1$ the curvature before rupture, and for simplicity approximating the bending modulus ratio at low and hight curvature by $\kappa\left(H_{\mathrm{max}}\right)/\kappa(0) \approx 2/3$, we can write:

$$\kappa\left(H\right) = \kappa(0)\left(1 - \frac{1}{3}\frac{|H|}{H_{\mathrm{max}}}\right) \tag{4.3}$$

Using Equation 4.2 to obtain the energy per area $\epsilon(H)$:

$$\epsilon\left(H\right) = 2\kappa(0)H^2\left(1 - \frac{2}{9}\frac{|H|}{H_{\mathrm{max}}}\right) \tag{4.4}$$

This energy is a third order symmetric polynomial in H, with only one minimum, at zero, and two symmetric maximums; the positive maximum that follows before the slope becomes negative is beyond the rupture curvature H_{max} and thus is not reached in our simulations. For comparison, the mean curvature term in the Helfrich Hamiltonian is $2\kappa\left(H - H_0\right)^2$, thus quadratic and allows specifying a spontaneous mean curvature H_0.

Strikingly, while for stiffer bolalipids ($k_{\mathrm{bola}} = 1 k_{\mathrm{B}} T$) the U-shaped bolalipid fraction increased strongly over a short range of the mean membrane curvature ($H = 1/(2R)$), we only found a small relative change in the U-shaped bolalipid fraction of flexible bolalipid membranes ($k_{\mathrm{bola}} = 0$) (Fig. 4.1B). We then looked at the fraction of these U-shaped conformers that are on the outer layer of the cylinder, u_f^o (Fig. 4.2). For flexible bolalipids, we can find that there is no preference for the outer or inner layer: u_f^o follows the ratio of area of the outer layer to the sum of each layer's area:

$$u_f^o = \frac{1 + Hh}{(1 + Hh) + (1 - Hh)} = \frac{1 + Hh}{2} \tag{4.5}$$

For bolalipids at $k_{\mathrm{bola}} = 1\, k_{\mathrm{B}} T$, however, U-shaped conformers non-linearly saturate, with u_f^o reaching above 90% before rupture. We can interpret this trend as the membrane being unable to match the increasing area difference with a proportional lipid ratio between leaflets, thus leading to the saturation and eventual rupture due to reaching critical tension.

Taken together, the rigidity of bolalipid membranes is not only controlled by the molecular stiffness of their lipid constituents but also by the emerging geometry of the ensemble of lipids. Since membrane geometry and thus membrane rigidity will change upon membrane deformations this gives rise to plastic material properties.

4.2 Bridging the low and high curvature regime

Thus far, we probed the membrane bending modulus via the height fluctuation method (Chapter 2) and the simulated cylinder method (Section 4.1). The height fluctuation method

Δt	N	l_z	H	$\left\|\frac{P_x+P_y}{2P_z}\right\|$	κ
0.001	19457	120	(3.08+/-0.04)e-02	0.03+/-0.06	8.9+/-2.4
	10000	70	(3.447+/-0.004)e-02	0.03+/-0.05	8.4+/-1.1
		80	(3.923+/-0.008)e-02	0.04+/-0.04	8.1+/-0.6
	5000	40	(3.948+/-0.006)e-02	0.05+/-0.05	8.8+/-1.3
		50	(4.942+/-0.009)e-02	0.011+/-0.021	8.6+/-0.6
		60	(5.857+/-0.005)e-02	0.018+/-0.017	8.22+/-0.33
		70	(6.82+/-0.02)e-02	0.010+/-0.013	8.27+/-0.30
		80	(7.17+/-0.03)e-02	0.009+/-0.011	8.7+/-0.3
0.005	5000	90	(7.86+/-0.03)e-02	0.010+/-0.006	9.16+/-0.21
		96	(8.13+/-0.03)e-02	0.085+/-0.013	8.87+/-0.27

Table 4.1: Parameters and measurements for bilayer lipid cylinders. N is number of lipids.

Δt	N	l_z	H	$\left\|\frac{P_x+P_y}{2P_z}\right\|$	κ	u_f
0.001	19457	120	(3.024+/-0.004)e-02	0.06+/-0.08	9.2+/-1.6	0.534+/-0.006
	10000	70	(3.354+/-0.004)e-02	0.03+/-0.08	9.7+/-2.1	0.536+/-0.004
		80	(3.848+/-0.004)e-02	0.04+/-0.05	9.5+/-1.4	0.537+/-0.005
	5000	40	(3.907+/-0.006)e-02	0.04+/-0.07	9.6+/-2.0	0.531+/-0.004
		50	(4.821+/-0.004)e-02	0.03+/-0.04	9.7+/-1.0	0.542+/-0.005
		60	(5.672+/-0.006)e-02	0.021+/-0.024	9.3+/-0.6	0.544+/-0.005
		70	(6.35+/-0.02)e-02	0.020+/-0.018	9.2+/-0.5	0.546+/-0.005
		80	(7.19+/-0.03)e-02	0.008+/-0.012	9.1+/-0.4	0.551+/-0.005
0.005	5000	90	(7.82+/-0.03)e-02	0.095+/-0.007	9.70+/-0.16	0.5583+/-0.0015
		96	(8.13+/-0.03)e-02	0.088+/-0.012	9.35+/-0.28	0.563+/-0.004

Table 4.2: Parameters and measurements for flexible bolalipids cylinders.

Δt	N	l_z	H	$\left\|\frac{P_x+P_y}{2P_z}\right\|$	κ	u_f
0.001	19457	120	(2.921+/-0.006)e-02	0.020+/-0.032	23.3+/-2.1	0.07401+/-0.00033
	10000	70	(3.260+/-0.002)e-02	0.043+/-0.028	23.3+/-1.7	0.0806+/-0.0009
		80	(3.743+/-0.002)e-02	0.021+/-0.022	22.0+/-1.5	0.0898+/-0.0009
	5000	50	(4.526+/-0.003)e-02	0.009+/-0.022	19.5+/-1.0	0.1053+/-0.0010
		60	(5.375+/-0.004)e-02	0.010+/-0.015	17.8+/-0.5	0.1225+/-0.0008

Table 4.3: Parameters and measurements for stiff bolalipid cylinders at $k_{\mathrm{bola}} = 1\, k_{\mathrm{B}}\, T$.

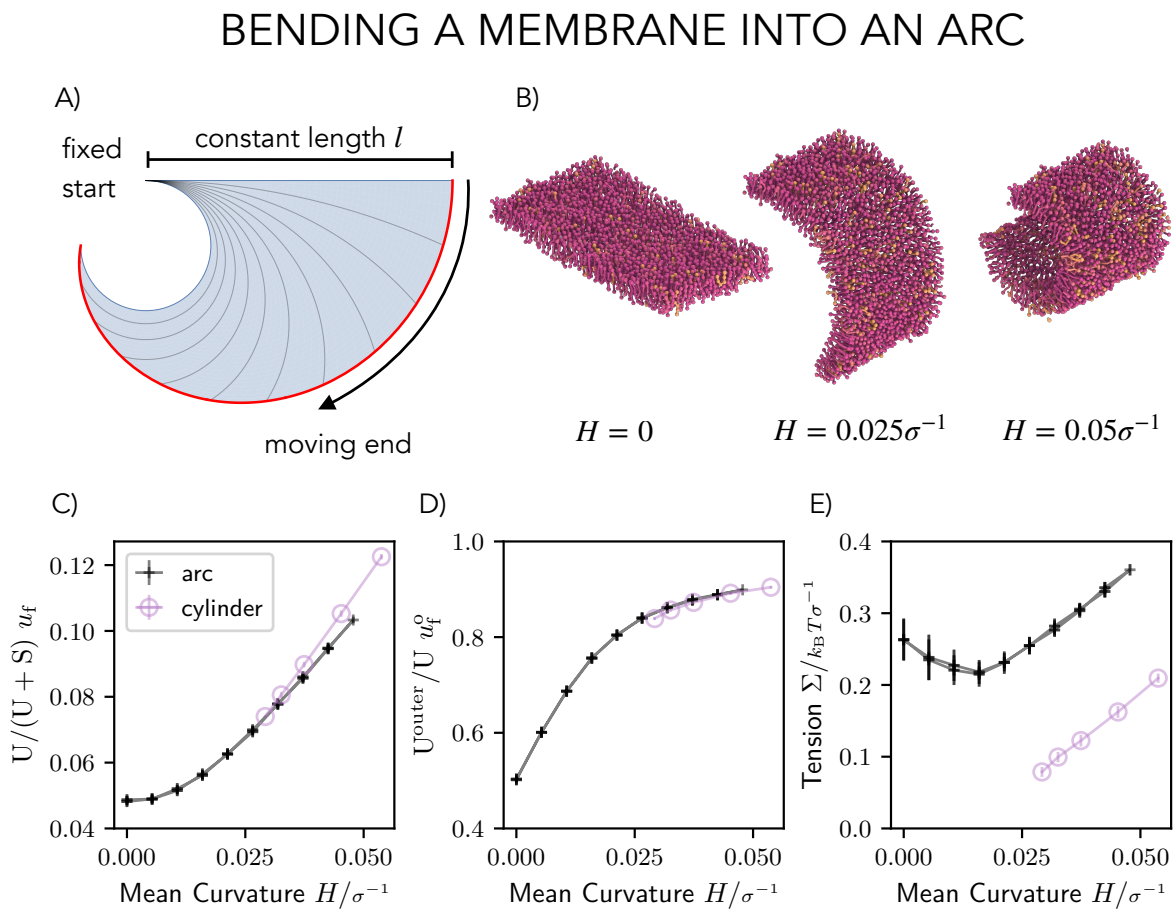

Figure 4.3: **Structure and mechanics of a bolalipid membrane arc.** (A) Schematic of the arc membrane shape (black lines) for different positions of the arc end (red line), and snapshots (B) for chosen values of mean curvature H, with bolalipids and respective head beads coloured according to conformation. We compare measurements of bolalipid conformation (C), U-shape location (D) and membrane tension obtained by bending a membrane into an arc (black lines) against the results obtained by simulating cylinders in Section 4.1 (purple lines). All data for membrane arcs is plotted in sequence of increasing then decreasing curvature, showing no significant hysteresis.

relies on analyzing the thermal fluctuations of a flat membrane patch, which in practice deform only by

$$\left\langle H^2 \right\rangle^{1/2} = \frac{1}{2L}\sqrt{\frac{k_\mathrm{B}T}{\kappa}} \tag{4.6}$$

which for our simulations reached at most the mean curvature of $H = 0.005\sigma^{-1}$. The cylinder method can simulate extreme curvatures, up to the point of either membrane rupture or near self-contact of the interior layer of the membrane. However, the membrane area required for the cylinder method grows as $1/H^2$: the radius of the cylinder scales as $1/H$ and its length needs to be scaled proportionally to impede fluctuations in the cross-section shape that would move the membrane away from the cylindrical ground state. Therefore, in our cylinder simulations we could not in practical time sample mean curvatures H below $0.025\sigma^{-1}$. To sample the intermediate curvature regime, we tested a protocol that takes a rectangular membrane patch and bends it into a membrane arc (Fig. 4.3A).

Simulation Protocol. We construct a membrane arc by taking a rectangular membrane, equilibrated at a small negative tension so that fluctuations are minimal. Then we remove the membrane that crosses the x-axis periodic boundaries, and freeze the positions of the resulting endpoints. This freezing of the particles positions is expected to stretch the membrane, since it essentially removes the compression effect of the endpoints momenta. We change the curvature by moving one of the endpoints so that the fictitious arc of constant curvature connecting both endpoints remains at constant length. By keeping arc length constant we expect to be near the same conditions as an equivalent arc section of a cylindrical membrane. We alternate between movement of the endpoint, over $10 \times 10^3\,\tau$, and equilibration at a fixed position for the same amount of simulation time, and perform the protocol first from zero curvature to maximum curvature, and then back to zero curvature, so we can check for hysteresis. To correct for the systematic contribution of the endpoints, which maintain the same conformation during the entire sequence of curvatures, we repeated the simulations and averaged over 20 different seeds.

Analysis. To be able to approximate the midplane and thus locate particles to the outer or inner layer of the membrane, we first transform the particle coordinates to arc coordinates (s, y, h) where s is length along the arc, y is unchanged and h is distance to the arc. In this coordinate system we then bin in (s, y), with a bind width of 3σ, and average h for each cell to obtain h_{m}, the midplane height. We compute the membrane tension $\Sigma = \frac{1}{l}\left\langle \sigma_{yy} L_x L_y L_z \right\rangle$, where L_i are the simulation box dimensions and l is the membrane arc length.

Results. Qualitatively, the shape of the membrane is well-described by an arc for most of the range of deformation (Fig. 4.3B). We also note that we observed no hysteresis in all measurements, likely because we allowed the membrane sufficient time to equilibrate between changes of curvature. Interestingly, regarding membrane structure there are two complementary trends. First, the fraction of U-shaped conformers u_{f} (Fig. 4.3C) is first slow to increase before steadily increasingly linearly with mean curvature H. Correspondingly, the fraction of U-shapes in the outer layer u_f^o is at first linear in mean curvature, as expected from a conformation with no preference for the outer or inner layer, and then saturates near 90%. We can interpret these results as the membrane first flip-flopping the existing reservoir of U-shaped conformers in the inner layer to match the growing area difference, and then only after exhausting it, forcing further bolalipids to take the U-shaped conformation. Unfortunately, because the membrane was pre-stressed to reduce fluctuations, and then had its endpoints frozen resulting in a sudden increase in tension, it is not surprising they do not match those made in cylinders at the same curvature (Fig. 4.3E). This makes it difficult to connect the tension measurements to the bending modulus, since we would need to account for this difference in the theory. This could be remedied, for instance, by dynamically controlling the box width L_y in such a way as to keep the membrane in an arc shape: extending it if the membrane is buckling, compressing it the membrane is stretched between its endpoints.

4.3 Tension is coupled to conformation

In our cylinder membrane and arc membrane simulations, we observed the U-shaped bolalipid conformers increase in fraction as the membrane was curved, and preferentially move to the outer layer for stiff bolalipids ($k_{\mathrm{bola}} = 1\,k_{\mathrm{B}}T$). In such a curved membrane, the curvature of the inner layer is higher than that of the outer layer, so there is an incentive to move lipid to the outer layer. At the same time, each layer's tension will counteract this movement,

resulting in a compressed outer layer and a stretched inner layer. However, since curving the membrane in both these configurations effectively increased tension, we were left with the question of how much of the conformation change was driven by area difference, versus being driven by tension. In fact, U-shaped lipids with $k_{\mathrm{bola}} > 0$, by virtue of having a preference to relax their conformation angle θ, will occupy more space in a membrane than straight conformations. Then whenever tension is positive it will be possible to partially relax it by increasing the number of U-conformers. Henceforth, we set up simulations of flat membrane patches that we then equilibrated at different values of projected area per head $a_{\mathrm{h}} = \frac{L_x L_y}{N_h}$, effectively replicating in part the pore formation setup from [17], but expecting to see novel behaviour.

Simulation & Analysis Protocol. We pre-assembled membranes as described in Chapter 2 in periodic simulation boxes with lateral size $L = 25\sigma$. We also controlled for finite size effects by simulating at $L = 50\sigma$, and since the trends observed were the same, we do not show data for these larger boxes. All measurements are averaged over four seeds. We picked the number of lipids such that we would exactly have a target projected area per head $a_{\mathrm{h,p}} = L^2/N_h$, where N_h is the number of lipid heads. We then simulated for $20 \times 10^3\,\tau$, discarding the first $1 \times 10^3\,\tau$ of the trajectory for equilibration. Anticipating the formation of pores at high enough $a_{\mathrm{h,p}}$, we measured the fraction of U-shapes u_{f} excluding any lipids near any found pores. To be able to track the buckling of the membrane under compression separately from tension, we also measured the R.M.S. area weighted average mean curvature $\langle H^2 \rangle$, using the method described in Chapter 3, optimized for the simpler flat geometry. In fact, we could obtain the signed distance of each bead to the membrane mid-surface, and thus compute a density profile with minimal noise induced by membrane fluctuations, to then inspect for structural responses to stretching.

Results. For bilayer membranes, the behaviour observed in terms of tension versus projected area per head (Fig. 4.4A) is as expected and described for the Cooke model in [17]: when the area per head is low enough, the membrane buckles to release compression, and, as the area per head is increased, the membrane transitions from compression (negative tension) to extension (positive tension), up to a critical value where a pore forms relaxing the tension partially. For bolalipid membranes, if the lipids are flexible and can acquire the U-shape conformation at no cost ($k_{\mathrm{bola}} = 0$), the behaviour is entirely similar and even agrees quantitatively. For stiff bolalipids, surprisingly, the compression regime is wider and reaches lower values of tension than bilayer membranes. The fraction of U-shaped conformers (Fig. 4.4B) nearly doubles in this regime and in general follows the same trend as tension. According to Section 4.1 findings on cylinder membranes, we can understand why buckling promotes U-shaped bolalipids. However, we can interpret the kink in tension at $a_{\mathrm{h,p}} = 1.2\sigma^2$, and to a lesser degree the inflection at the same coordinate that happens in curvature (Fig. 4.4C), to mark the end of buckling. Thus, the membrane promotion of U-shapes that happens during compression and stretching cannot be curvature-related, and thus shows that U-shapes are promoted due to occupying a larger volume per bead in the membrane compared to straight shapes. In fact, U-shapes, by virtue of relaxing their central angle potentials, will likely distance their head beads and thus have attain a smaller thickness to match that of straight bolalipids.

To inspect the behaviour of the membrane structure in regard to stretching, we computed the average density profiles for our membranes (Fig. 4.5). This also allowed us to quantitatively verify our assumptions about the location of lipid species and bolalipid conformations in relation to the membrane mid-surface. We corrected for fluctuations by computing these

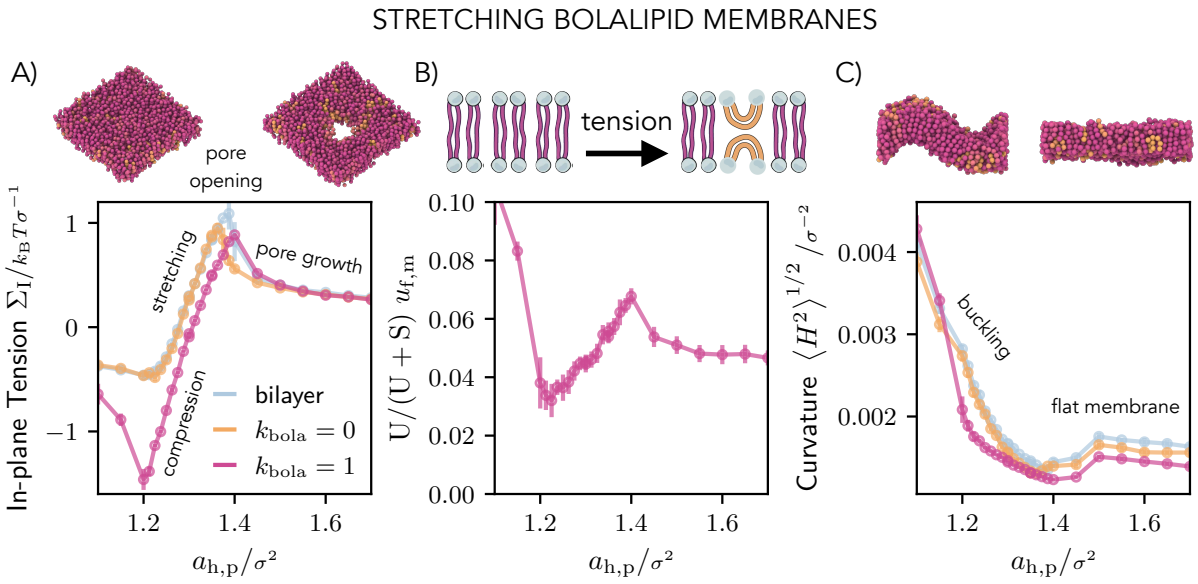

Figure 4.4: **Structure and mechanics of membranes under tension.** (A) Tension versus projected area per head for bilayer membrane, flexible bolalipids ($k_{\rm bola}=0$) and stiff bolalipids ($k_{\rm bola}=1\,k_{\rm B}\,T$), showing the same trend corresponding to the sequence of buckling, stretching, pore formation and pore growth. For the stiff bolalipids there is a clear positive correlation of between the fraction of U-shaped conformers and tension (B), that cannot be explained by membrane curvature (C), which has the opposite trend.

profiles relative to the membrane surface, and further avoided their influence by choosing $a_{\rm h,p}$ past the buckling region. Straight bolalipids do fill the void normally present at the centre of bilayer membranes. We could confirm that the membrane compresses in the vertical direction when it stretches, with density varying by as much as (15%). Curiously, for flexible bolalipids while the fraction of U-shape conformers on first analysis did not show any appreciable trend (thus we do not show it), we could discern through the density profile that U-shape conformers were responsible for most of the density change in the outer region, as opposed to the core, where both conformations were relevant for increasing the density. In general, all membranes increase density in their centre when stretched.

4.4 Discussion

It is striking that membranes made from stiffer bolalipids showed a curvature-dependent bending modulus (Section 4.1), which is a clear signature that bolalipid membranes exhibit plastic behaviour during membrane reshaping. Since bolalipids in the U-shape conformation occupy more membrane volume than in the straight conformation (Section 4.3), a possible reason bolalipid membranes can soften as they are bent is that the promotion of U-shapes not only responds to the area difference, but also compresses the outer layer due to the conformation-change volume increase, which eases the bending of the membrane. This would not happen as much at low curvatures, since then there is a reservoir of U-shape conformers that can flip-flop (Section 4.2). Arguably, this curvature-dependent bending modulus is a qualitatively different solution to the stability versus flexibility trade-off than that presented by a bolalipid and bilayer lipid mixture (introduced in Section 2.4). Increasing the fraction of

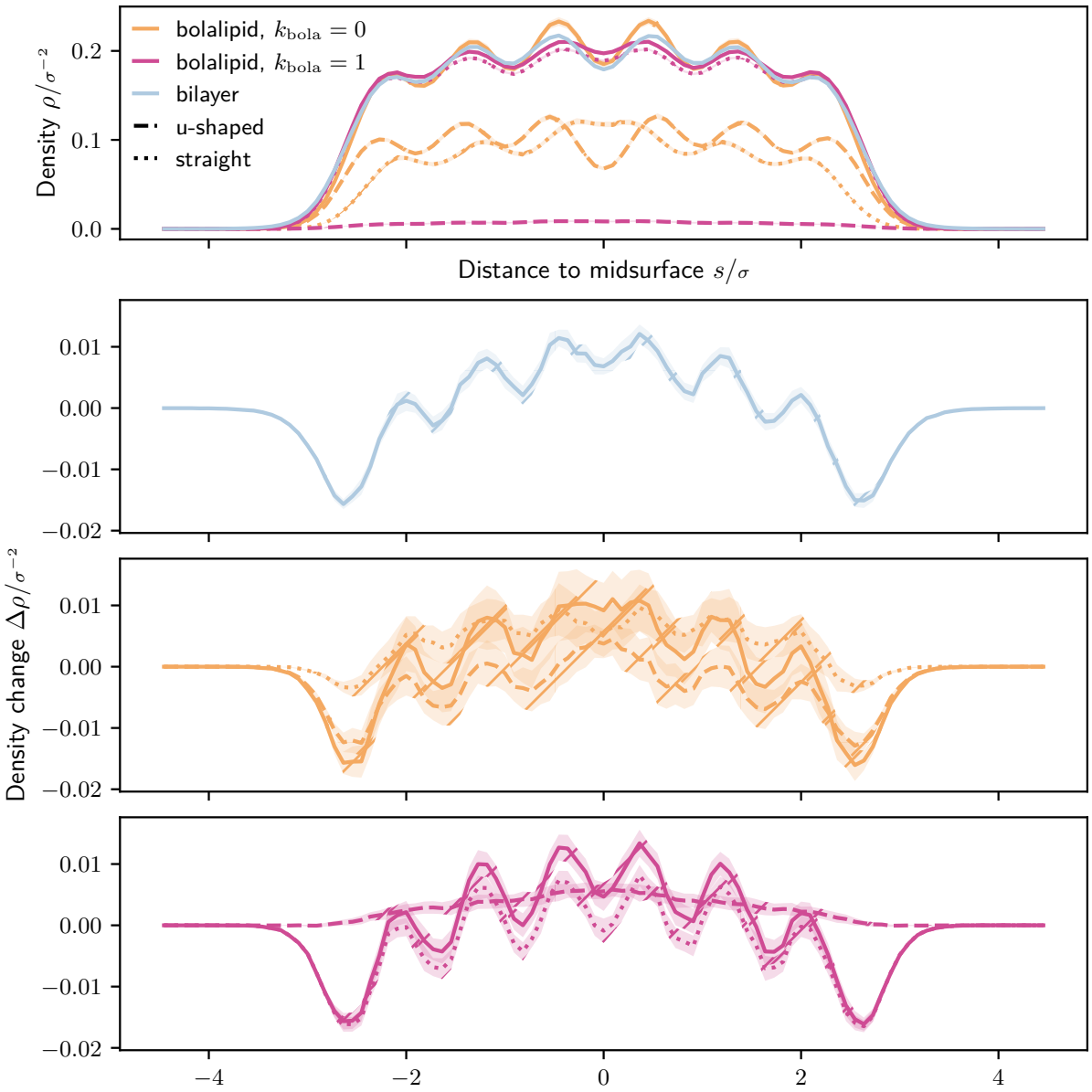

Figure 4.5: **Density profile for membranes under tension.** Reference density profile ρ_{ref} (top) for membranes, for bilayer membrane, flexible bolalipids ($k_{\mathrm{bola}} = 0$) and stiff bolalipids ($k_{\mathrm{bola}} = 1\, k_{\mathrm{B}}T$), at $a_{\mathrm{h,p}} = 1.25$. For bolalipid membranes we also plot separately the two conformations whose densities add up to the total density. Bilayer membranes have a distinctive 6-toothed profile, matching the number of beads in two bilayer lipids. This profile is shared by flexible bolalipids where it can be attributed to high fraction of U-shaped conformers. The central void at the membrane centre is missing for stiffer bolalipids ($k_{\mathrm{bola}} = 1\, k_{\mathrm{B}}T$), which fill it with straight conformers. We compare these profiles with those at higher area per head, thus at extension, by plotting the change $\Delta\rho = \rho - \rho_{\mathrm{ref}}$ at $a_{\mathrm{h,p}} = 1.34$, separately for each membrane (bottom three plots). For these plots shading is used instead of error bars. All membranes show a negative change near the boundary and positive on their core.

bilayer lipids in a bolalipid membrane lowers its bending rigidity making reshaping possible, however it simultaneously increases the diffusion factor of the membrane lipids, which we can interpret as decreasing its resistance to high temperature. Contrastingly, the stiff bolalipid membrane we analysed in this chapter have maximum rigidity at large scales (small curvature), and soften gradually once deformed to high curvature. This can be seen as the membrane imposing a barrier to large scale deformation, while allowing deformation at smaller scales at a lower energetic cost, without making concessions on temperature resistance.

CHAPTER 5

Conclusion and outlook

In this thesis we designed and performed the first detailed mechanical characterization of a coarse-grained model for archaeal membranes, containing bipolar lipids called bolalipids that can exist in two conformations. We covered both pure bolalipid membranes and membranes composed of a mixture of bilayer lipids and bolalipids. In Chapter 2, our coarse-grained molecular dynamics simulations show that the geometry of bolalipids is sufficient to shift the fluid phase of archaeal-type membranes so that they are stable at high temperatures. In addition, we show that by increasing bolalipids molecular rigidity (k_{bola}), membranes assembled from bolalipids can have a much higher bending rigidity than bilayer-derived membranes. We also show that mixing a small fraction ($\approx 10\%$) of bilayer lipids near their gas phase with bolalipids in their gel phase is sufficient to obtain a fully well-mixed liquid membrane with tunable rigidity and temperature resistance. In Chapter 3, we tested the ability of these membranes to both deform and change topology, by simulating cargo budding with a tunable membrane-cargo adsorption strength ϵ_{mc}. These simulations showed that during membrane deformation, stress in these bolalipid membranes can be relieved via a small fraction of bolalipids taking up a U-shaped conformation, which renders them a mechanically switchable material. If the molecular rigidity k_{bola} is too high, however, these conformations are forbidden, budding requires a higher critical adsorption energy ϵ^*_{mc}, and large pores form on the curved membrane bud. Remarkably, membrane mixtures of bilayer lipids and bolalipids budded successfully covering a similar range of required adsorption energy, without ever forming membrane pores. Finally, in Chapter 4, we explored curvature dependency of the bending modulus; while bilayer lipid membranes and flexible bolalipid membranes ($k_{\mathrm{bola}} = 0$) have a constant bending modulus, bolalipids with intermediate molecular rigidity form plastic membranes, in the sense that their bending modulus linearly decreases significantly (40%) over the range of allowed mean curvature.

Let us now take our work as a whole, and ask if, like real archaeal membranes, we achieved to solve the trade-off between flexibility and temperature resistance. In other words, we can consider an archaeal membrane design successful if it both can withstand higher temperatures than a bilayer membrane, while still being reshapeable, i.e. have a bending modulus close to that of the bilayer membrane. Given these criteria, we found two possible solutions. The first solution is a mixture of a small amount of bilayer lipids with rigid bolalipids. The bolalipids are all in the straight conformation and confer rigidity to the membrane, while fluidity can be attributed to the bilayer lipids. Consequently, varying the fraction of bilayer lipids allows one to have a continuous trade-off, where increasing the bilayer lipid fraction moves bending rigidity

closer to bilayer membrane values, while increasing fluidity and thus moving the membrane closer to the gas phase transition, thus lowering the tolerance to increases in temperature. The lipid mixture is supported by real biological archaeal membranes, where there is almost always some fraction of bilayer lipids [60] that is adjusted according to the cell growth environment, with bolalipids being favoured at higher temperature [45]. The second solution is a membrane made exclusively of bolalipids with moderate molecular rigidity, where around 5% of lipids acquire the U-shape conformation. We showed that the bolalipid conformation is tension sensitive, and that under curvature stress, this results in plastic behaviour, where the membrane softens as it is bent, with κ, the bending modulus, decreasing linearly by 40% from $\approx 30\, k_\mathrm{B}T$ to bilayer-like values of $\approx 20\, k_\mathrm{B}T$, going from a flat membrane to maximum curvature radius that is only slightly above the membrane thickness. This makes for a different mechanism for enduring high temperatures. When the membrane is relatively flat, i.e. with radius of curvature greater than $50\,\sigma \approx 50\,\mathrm{nm}$, the membrane is rigid and thus has reduced shape fluctuations; when it is sufficiently bent, the membrane yields, allowing for high curvature reshaping to occur at lower energetic cost. In support of the pure bolalipid solution, there is experimental evidence of almost pure ($> 99\%$ in lipid fraction) bolalipid membranes successfully undergoing fusion [10]. It would take further work on mapping real lipids to our coarse-grained model to determine the equivalent k_bola, so we cannot say at this moment if these experiments are better described by our flexible bolalipid membrane ($k_\mathrm{bola} = 0$), or by a moderately stiff membrane with fewer U-shape conformers ($k_\mathrm{bola} > 0$).

During our exploration of membrane designs, we inevitably left some directions unexplored. In Chapter 3, we simulated cargo wrapping and budding as an-all encompassing test containing both membrane deformation and topology change with a clear biological equivalent in trafficking and membrane fusion. To test our membrane mechanics characterization, we could attempt to quantitively match the observed values of critical adsorption energy to those predicted by theoretical analysis, given what we now know about membrane mechanics, since either we have measured or could now easily measure the bending modulus, the gaussian modulus and the line tension for our membranes. On the other hand, this analysis would certainly be complicated by the curvature dependent bending modulus that we observed for bolalipids of intermediate rigidity, since we would have to extrapolate from the measured range of mean curvature to the curvature experienced in the cargo bud, which is roughly twice that of the rupture mean curvature for bolalipids at $k_\mathrm{bola} = 1\, k_\mathrm{B}T$. Another difficulty is that above a certain membrane rigidity, which increases considerably with k_bola, we expect the method used for measuring the gaussian modulus to become impractical to apply, since it would require the simulation of prohibitively large partially curved membrane disks.

In this work we commented several times on membrane tension, in some cases by indirect observation via the area per lipid (Section 3.5), in others by relating it to the simulation box stress tensor (Sections 4.1 and 4.3). Further work could focus on connecting the emerging global tension to the composition and local structure of the membrane. Consider the cylinder simulations in Section 4.1 and the stretching simulations in Section 4.3. In both cases we compute the simulation stress tensor, which in practice is done by summing the per-particle stress tensor over all particles. We could instead group particles by lipid species and conformation, to obtain the respective contribution from each component. Additionally, for each of these components we could obtain stress profiles by binning each contribution according to the signed distance to the membrane midsurface. This kind of stress profile computation is readily implemented in software packages like LAMMPS for both fixed cylindrical and planar geometries, which in less coarse-grained simulations are a good approximation of the membrane shape [43]. However, since our simulations develop significant shape fluctuations, we would

benefit from using our current membrane midplane fitting procedure to reduce measurement noise, as we did in Section 4.3 for our density profiles. Computing these stress profiles would enable us to measure the stress in each leaflet and check our current hypothesis that bolalipid U-shape conformers contribute more to tension than straight conformers.

In Section 4.2, we intended to capture membrane structure and mechanics as it was continuously deformed from flat to a high curvature state. Essentially, it is an attempt at simulation only a section of a cylinder, with constant arc length, to make it possible to simulate in practical time a membrane at low curvatures, since this regime for the usual cylinder method was prohibitively expensive and noisy due to large shape fluctuations. However, for arc membranes the membrane tension behaviour was different from that of cylinder membranes at low curvatures. For continuing this work, we propose two directions. First, the implementation of an active control of the radius of the arc or 'arc-stat', imposed by the fixed membrane edges: by computing the membrane shape deviation from an arc, it should be possible to determine if it is currently below the arc, thus stretched, and consequently reduce the arc radius to compress it; vice-versa for when the membrane has buckled above the intended arc shape. Secondly, instead of freezing the membrane edges to impose the arc shape, one can go down the technically difficult route of implementing periodic boundary conditions at an angle. This would let particles cross from one end of the arc to the other, and for the membrane to freely chose an equilibrium radius, dispensing with the need for an active shape control. While implementing this concept in the mature simulator LAMMPs would be a considerable chunk of work, we successfully managed to test it for a LJ gas on the less complex jax-md [49] simulation package, by changing how neighbour lists, velocity updates and position deltas were computed.

Alternatively, we could buckle a thin strip of membrane by compressing it along its length, allowing for a wide range of mean curvatures to be sampled, following the method in [20]. However, since this method creates membranes with varying curvature along their length, it would necessarily complicate our analysis. Now that we are on more solid footing regarding the membrane behaviour w.r.t. to mean curvature, we could use this method to fill in the bending modulus for the low curvature range. More importantly, since a gradient of curvature induces tilt, this method can also observe static lipid tilt and measure the tilt modulus [63], thus providing a second avenue to supplement our membrane height fluctuation spectrums fits that indicated the presence of lipid tilting (Chapter 2). Because it would be a static observation of tilt, this would likely provide a more convincing path than further analysis of the fluctuation simulations, for which we could compute the tilt field and from a fit to its spectrum obtain the tilt modulus, like done in [22].

As a variation on our model, one could replace the harmonic angle potentials in the central part of bolalipids by a double well potential. By tuning the energy barrier separately from the steepness of the wells, the energy cost of U-shape formation would be tunable independently of the in-leaflet preferred curvature or induced stress of a U-shape, allowing the exploration of regimes such as both high U-shape fraction and high U-shape induced stress, or low U-shape fraction with negligible U-shape induced curvature.

While our simulations have provided significant insights, several paths remain open for further exploration. Our simulations indicated that mixing bilayer lipids with bolalipids results in a flexible membrane, however it incurs a cost in terms of lower temperature tolerance and increased permeability. While there is previous experimental work [62] on mixtures of non-branched bilayer lipids and archaeal bolalipids (henceforth, with branched tails), the mismatch between the type of tails makes it difficult to map the results to our model. Therefore, a

promising area for experimental investigation is that of the properties of membrane mixtures of archaeal bilayer lipids and bolalipids. This exploration could validate our simulation predictions about the trade-off between membrane flexibility, temperature tolerance and porosity, and contribute to our understanding of how archaea adjust their membrane composition in response to temperature changes. Understanding this relationship could also be useful for applications that require precise control over membrane permeability in extreme conditions, such as in the development of selective barriers or channels in synthetic biology.

To validate the effects of tuning the bolalipid rigidity k_{bola}, we would benefit from experimental research into how the number of cyclopentane rings in bolalipids affects membrane properties. Bolalipids with more cyclopentane rings are expected to have increased molecular rigidity, which our simulation shows can significantly affect membrane properties, such as the bending modulus and temperature stability. Confirming these predictions would validate our model and open the way for a composition-tunable wide range of membrane rigidities. For membranes of bolalipids of moderate rigidity $k_{\mathrm{bola}} > 0$, we observed a curvature-dependent bending modulus. Consequently, it would be of interest to experimentally characterize the mechanical properties of membranes across different curvature regimes. By controlling and fixing membrane tension during tether extrusion, it should be possible to obtaining tethers of different radii, and thus measure the corresponding bending modulus as a function of curvature, mimicking our cylinder experiments. By regulating both molecular rigidity and measuring membrane mechanics at both low and high curvature, we would be able to have a direct comparison with our simulation results. To get to the likely root cause of this behaviour, it would be helpful to see development in methods to detect and quantify the amount of U-shape conformers in membranes, which would make it possible to determine whether these conformations are enriched by bending or stretching.

Generalizing, our findings on bolalipids with intermediate molecular rigidity suggest the possibility of synthesizing plastic membranes composed of components that can flip-flop between conformations sensitive to tension. Research into creating such membranes could lead to materials with programmable mechanical responses, where the bending modulus is curvature-dependent - a property we observed in our simulations. These membranes could have applications in biotechnology and nanotechnology, where controllable membrane mechanics are desirable. In conclusion, our work lays a foundation for future studies aimed at bridging computational predictions and experimental observations. By further exploring the mechanical properties of archaeal membranes and their dependence on lipid composition and conformation, we can deepen our understanding of membrane biology. This research not only contributes to fundamental biological knowledge but also has the potential to inspire the development of novel biomimetic materials with tailored properties for a range of technological applications. We look forward to seeing how these explorations unfold, potentially guiding both theoretical models and experimental designs in the field of membrane biophysics.

Bibliography

[1] Sonja-Verena Albers and Benjamin H. Meyer. "The Archaeal Cell Envelope". In: *Nature Reviews Microbiology* 9.6 (May 2011), pp. 414–426. ISSN: 1740-1534. DOI: 10.1038/nrmicro2576. PMID: 21572458.

[2] Miguel Amaral. *Archaeal_membranes : Code and Examples*. Zenodo. Oct. 2024. DOI: 10.5281/zenodo.13934991.

[3] Miguel Amaral et al. *Stability vs Flexibility: Reshaping Monolayer and Bilayer Archaeal Membranes in Silico*. Oct. 2024. DOI: 10.1101/2024.10.18.619072.

[4] Brett J. Baker et al. "Diversity, Ecology and Evolution of Archaea". In: *Nature Microbiology* 5.7 (July 2020), pp. 887–900. ISSN: 2058-5276. DOI: 10.1038/s41564-020-0715-z.

[5] U Bakowsky et al. "Monomolecular Organization of the Main Tetraether Lipid from Thermoplasma Acidophilum at the Water–Air Interface". In: *Chemistry and Physics of Lipids* 105.1 (Mar. 2000), pp. 31–42. DOI: 10.1016/s0009-3084(99)00131-0.

[6] Andrew J. Balchunas et al. "Equation of State of Colloidal Membranes". In: *Soft Matter* 15.34 (2019), pp. 6791–6802. ISSN: 1744-683X, 1744-6848. DOI: 10.1039/c9sm01054h.

[7] Edward Barry and Zvonimir Dogic. "Entropy Driven Self-Assembly of Nonamphiphilic Colloidal Membranes". In: *Proceedings of the National Academy of Sciences* 107.23 (May 2010), pp. 10348–10353. ISSN: 0027-8424, 1091-6490. DOI: 10/bj8jp8.

[8] Oleg V. Batishchev et al. "Cyclopentane Rings in Hydrophobic Chains of a Phospholipid Enhance the Bilayer Stability to Electric Breakdown". In: *Soft Matter* 16.13 (2020), pp. 3216–3223. ISSN: 1744-683X, 1744-6848. DOI: 10.1039/c9sm02001b.

[9] David A Baum and Buzz Baum. "An Inside-out Origin for the Eukaryotic Cell". In: *BMC Biology* 12.1 (Dec. 2014), p. 76. ISSN: 1741-7007. DOI: 10.1186/s12915-014-0076-2.

[10] Ahanjit Bhattacharya et al. "Structure–Function Relationships in Pure Archaeal Bipolar Tetraether Lipids". In: *Chemical Science* 15.35 (Sept. 2024), pp. 14273–14286. ISSN: 2041-6539. DOI: 10.1039/D4SC03788J.

[11] David P. Brownholland et al. "Phase Separation in Binary Mixtures of Bipolar and Monopolar Lipid Dispersions Revealed by 2H NMR Spectroscopy, Small Angle X-Ray Scattering, and Molecular Theory". In: *Biophysical Journal* 97.10 (Nov. 2009), pp. 2700–2709. ISSN: 0006-3495. DOI: 10.1016/j.bpj.2009.06.058.

[12] Monica Bulacu, Xavier Périole, and Siewert J. Marrink. "In Silico Design of Robust Bolalipid Membranes". In: *Biomacromolecules* 13.1 (Jan. 2012), pp. 196–205. ISSN: 1525-7797, 1526-4602. DOI: 10.1021/bm201454j.

[13] E.L. Chang. "Unusual Thermal Stability of Liposomes Made from Bipolar Tetraether Lipids". In: *Biochemical and Biophysical Research Communications* 202.2 (July 1994), pp. 673–679. ISSN: 0006291X. DOI: 10.1006/bbrc.1994.1983.

[14] Parkson Lee-Gau Chong. "Archaebacterial Bipolar Tetraether Lipids: Physico-chemical and Membrane Properties". In: *Chemistry and Physics of Lipids* 163.3 (Mar. 2010), pp. 253–265. ISSN: 00093084. DOI: 10/c3kzbg.

[15] Parkson Lee-Gau Chong et al. "On Physical Properties of Tetraether Lipid Membranes: Effects of Cyclopentane Rings". In: *Archaea* 2012 (2012), pp. 1–11. ISSN: 1472-3646, 1472-3654. DOI: 10.1155/2012/138439.

[16] Anton O. Chugunov et al. "Liquid but Durable: Molecular Dynamics Simulations Explain the Unique Properties of Archaeal-Like Membranes". In: *Scientific Reports* 4.1 (Dec. 2014), pp. 1–8. ISSN: 2045-2322. DOI: 10.1038/srep07462.

[17] Ira R. Cooke and Markus Deserno. "Solvent-Free Model for Self-Assembling Fluid Bilayer Membranes: Stabilization of the Fluid Phase Based on Broad Attractive Tail Potentials". In: *The Journal of Chemical Physics* 123.22 (Dec. 2005), p. 224710. ISSN: 0021-9606, 1089-7690. DOI: 10.1063/1.2135785.

[18] Markus Deserno. "Elastic Deformation of a Fluid Membrane upon Colloid Binding". In: *Physical Review E* 69.3 (Mar. 2004), p. 031903. DOI: 10.1103/PhysRevE.69.031903.

[19] Markus Deserno. "Fluid Lipid Membranes: From Differential Geometry to Curvature Stresses". In: *Chemistry and Physics of Lipids* 185 (Jan. 2015), pp. 11–45. ISSN: 00093084. DOI: 10.1016/j.chemphyslip.2014.05.001.

[20] Patrick Diggins and Markus Deserno. "Determining the Bending Modulus of a Lipid Membrane by Simulating Buckling". In: *The Journal of Chemical Physics* 138.21 (June 2013), p. 214110. ISSN: 0021-9606, 1089-7690. DOI: 10.1063/1.4808077.

[21] Z DOGIC and S FRADEN. "Ordered Phases of Filamentous Viruses". In: *Current Opinion in Colloid & Interface Science* 11.1 (Apr. 2006), pp. 47–55. ISSN: 13590294. DOI: 10.1016/j.cocis.2005.10.004.

[22] Muhammed F. Ergüder and Markus Deserno. "Identifying Systematic Errors in a Power Spectral Analysis of Simulated Lipid Membranes". In: *The Journal of Chemical Physics* 154.21 (June 2021), p. 214103. ISSN: 0021-9606. DOI: 10.1063/5.0049448.

[23] Felix Frey and Timon Idema. "More than Just a Barrier: Using Physical Models to Couple Membrane Shape to Cell Function". In: *Soft Matter* 17.13 (2021), pp. 3533–3549. ISSN: 1744-683X, 1744-6848. DOI: 10.1039/d0sm01758b.

[24] Timur R. Galimzyanov et al. "Elastic Deformations of Bolalipid Membranes". In: *Soft Matter* 12.8 (2016), pp. 2357–2364. ISSN: 1744-683X, 1744-6848. DOI: 10.1039/c5sm02635k.

[25] D W Grogan. "Phenotypic Characterization of the Archaebacterial Genus Sulfolobus: Comparison of Five Wild-Type Strains". In: *Journal of Bacteriology* 171.12 (Dec. 1989), pp. 6710–6719. DOI: 10.1128/jb.171.12.6710-6719.1989.

[26] Annette Gulik et al. "Structure and Polymorphism of Bipolar Isopranyl Ether Lipids from Archaebacteria". In: *Journal of Molecular Biology* 182.1 (Mar. 1985), pp. 131–149. ISSN: 00222836. DOI: 10.1016/0022-2836(85)90032-4.

[27] M. Hamm and M.M. Kozlov. "Elastic Energy of Tilt and Bending of Fluid Membranes". In: *The European Physical Journal E* 3.4 (Dec. 2000), pp. 323–335. ISSN: 1292-8941. DOI: 10.1007/s101890070003.

[28] Vagelis A. Harmandaris and Markus Deserno. "A Novel Method for Measuring the Bending Rigidity of Model Lipid Membranes by Simulating Tethers". In: *The Journal of Chemical Physics* 125.20 (Nov. 2006), p. 204905. ISSN: 0021-9606, 1089-7690. DOI: 10/bzx6xs.

[29] W Helfrich. "Elastic Properties of Lipid Bilayers: Theory and Possible Experiments". In: *Zeitschrift für Naturforschung C* 28.11-12 (Dec. 1973), pp. 693–703. ISSN: 1865-7125, 0939-5075. DOI: 10.1515/znc-1973-11-1209.

[30] Amirali Hossein and Markus Deserno. "Spontaneous Curvature, Differential Stress, and Bending Modulus of Asymmetric Lipid Membranes". In: *Biophysical Journal* 118.3 (Feb. 2020), pp. 624–642. ISSN: 00063495. DOI: 10.1016/j.bpj.2019.11.3398.

[31] Mingyang Hu, John J. Briguglio, and Markus Deserno. "Determining the Gaussian Curvature Modulus of Lipid Membranes in Simulations". In: *Biophysical Journal* 102.6 (Mar. 2012), pp. 1403–1410. ISSN: 00063495. DOI: 10.1016/j.bpj.2012.02.013.

[32] Carme Huguet et al. "Molecular Dynamics Simulation Study of the Effect of Glycerol Dialkyl Glycerol Tetraether Hydroxylation on Membrane Thermostability". In: *Biochimica et Biophysica Acta (BBA) - Biomembranes* 1859.5 (May 2017), pp. 966–974. ISSN: 00052736. DOI: 10.1016/j.bbamem.2017.02.009.

[33] Christoph Jeworrek et al. "Structure and Phase Behavior of Archaeal Lipid Monolayers". In: *Langmuir* 27.21 (Oct. 2011), pp. 13113–13121. ISSN: 0743-7463. DOI: 10.1021/la202027s.

[34] Young Hun Kim et al. "Entropic Effects Enable Life at Extreme Temperatures". In: *Science Advances* 5.5 (May 2019), eaaw4783. ISSN: 2375-2548. DOI: 10.1126/sciadv.aaw4783.

[35] Urszula apiska et al. "Systematic Comparison of Unilamellar Vesicles Reveals That Archaeal Core Lipid Membranes Are More Permeable than Bacterial Membranes". In: *PLOS Biology* 21.4 (Apr. 2023), e3002048. ISSN: 1545-7885. DOI: 10.1371/journal.pbio.3002048.

[36] Geraldy Lie Stefanus Liman et al. "Tetraether Archaeal Lipids Promote Long-term Survival in Extreme Conditions". In: *Molecular Microbiology* (Feb. 2024), p. mmi.15240. ISSN: 0950-382X, 1365-2958. DOI: 10.1111/mmi.15240.

[37] Edward Lyman and Alexander J. Sodt. "Differential or Curvature Stress? Modus Vivendi". In: *Biophysical Journal* 118.3 (Feb. 2020), pp. 535–537. ISSN: 00063495. DOI: 10.1016/j.bpj.2019.11.3399.

[38] Eric R. May, Atul Narang, and Dmitry I. Kopelevich. "Role of Molecular Tilt in Thermal Fluctuations of Lipid Membranes". In: *Physical Review E* 76.2 (Aug. 2007), p. 021913. DOI: 10.1103/physreve.76.021913.

[39] Harvey T. McMahon and Jennifer L. Gallop. "Membrane Curvature and Mechanisms of Dynamic Cell Membrane Remodelling". In: *Nature* 438.7068 (Dec. 2005), pp. 590–596. ISSN: 0028-0836, 1476-4687. DOI: 10.1038/nature04396.

[40] Hiroshi Noguchi. "Membrane Simulation Models from Nanometer to Micrometer Scale". In: *Journal of the Physical Society of Japan* 78.4 (Apr. 2009), p. 041007. ISSN: 0031-9015, 1347-4073. DOI: 10.1143/jpsj.78.041007.

[41] Philippe M. Oger and Anaïs Cario. "Adaptation of the Membrane in Archaea". In: *Biophysical Chemistry* 183 (Dec. 2013), pp. 42–56. ISSN: 03014622. DOI: 10.1016/j.bpc.2013.06.020.

[42] Rob Phillips et al. *Physical Biology of the Cell*. Garland Science, New York, 2012.

[43] Konstantin V. Pinigin. "Local Stress in Cylindrically Curved Lipid Membrane: Insights into Local Versus Global Lateral Fluidity Models". In: *Biomolecules* 14.11 (Nov. 2024), p. 1471. ISSN: 2218-273X. DOI: 10.3390/biom14111471.

[44] T. Pomorski and A. K. Menon. "Lipid Flippases and Their Biological Functions". In: *Cellular and Molecular Life Sciences CMLS* 63.24 (Dec. 2006), pp. 2908–2921. ISSN: 1420-9071. DOI: 10.1007/s00018-006-6167-7.

[45] Julian Quehenberger et al. "The Influence of the Specific Growth Rate on the Lipid Composition of Sulfolobus Acidocaldarius". In: *Extremophiles* 24.3 (May 2020), pp. 413–420. ISSN: 1433-4909. DOI: 10.1007/s00792-020-01165-1.

[46] Kerstin Rastädter et al. "The Cell Membrane of Sulfolobus Spp.—Homeoviscous Adaption and Biotechnological Applications". In: *International Journal of Molecular Sciences* 21.11 (May 2020), p. 3935. DOI: 10.3390/ijms21113935.

[47] Tomá ezanka, Lucie Kyselová, and Denis J. Murphy. "Archaeal Lipids". In: *Progress in Lipid Research* 91 (July 2023), p. 101237. ISSN: 0163-7827. DOI: 10.1016/j.plipres.2023.101237.

[48] Mohsen Sadeghi and Frank Noé. "Hydrodynamic Coupling for Particle-Based Solvent-Free Membrane Models". In: *The Journal of Chemical Physics* 155.11 (Sept. 2021), p. 114108. ISSN: 0021-9606, 1089-7690. DOI: 10.1063/5.0061623.

[49] Samuel S. Schoenholz and Ekin D. Cubuk. "JAX M.D. a Framework for Differentiable Physics". In: *Advances in Neural Information Processing Systems*. Vol. 33. Curran Associates, Inc., 2020.

[50] Stefan Schouten et al. "Widespread Occurrence of Structurally Diverse Tetraether Membrane Lipids: Evidence for the Ubiquitous Presence of Low-Temperature Relatives of Hyperthermophiles". In: *Proceedings of the National Academy of Sciences* 97.26 (Dec. 2000), pp. 14421–14426. DOI: 10.1073/pnas.97.26.14421.

[51] Thomas B.H. Schroeder et al. "Effects of Lipid Tethering in Extremophile-Inspired Membranes on H + /OH - Flux at Room Temperature". In: *Biophysical Journal* 110.11 (June 2016), pp. 2430–2440. DOI: 10.1016/j.bpj.2016.04.044.

[52] Udo Seifert. "Configurations of Fluid Membranes and Vesicles". In: *Advances in Physics* 46.1 (Feb. 1997), pp. 13–137. ISSN: 0001-8732, 1460-6976. DOI: 10.1080/00018739700101488.

[53] Melvin F. Siliakus, John van der Oost, and Servé W. M. Kengen. "Adaptations of Archaeal and Bacterial Membranes to Variations in Temperature, pH and Pressure". In: *Extremophiles* 21.4 (May 2017), pp. 651–670. ISSN: 1431-0651, 1433-4909. DOI: 10.1007/s00792-017-0939-x.

[54] Anja Spang et al. "Complex Archaea That Bridge the Gap between Prokaryotes and Eukaryotes". In: *Nature* 521.7551 (May 2015), pp. 173–179. ISSN: 1476-4687. DOI: 10.1038/nature14447.

[55] Christopher T Straub et al. "Biotechnology of Extremely Thermophilic Archaea". In: *FEMS Microbiology Reviews* 42.5 (June 2018), pp. 543–578. ISSN: 1574-6976. DOI: 10.1093/femsre/fuy012.

[56] Alexander Stukowski. "Visualization and Analysis of Atomistic Simulation Data with OVITO–the Open Visualization Tool". In: *Modelling and Simulation in Materials Science and Engineering* 18.1 (Dec. 2009), p. 015012. DOI: 10.1088/0965-0393/18/1/015012.

[57] M. Mert Terzi, Markus Deserno, and John F. Nagle. "Mechanical Properties of Lipid Bilayers: A Note on the Poisson Ratio". In: *Soft Matter* 15.44 (2019), pp. 9085–9092. ISSN: 1744-683X, 1744-6848. DOI: 10.1039/C9SM01290G.

[58] Courtney M. Thomas et al. "Factors Shaping the Abundance and Diversity of the Gut Archaeome across the Animal Kingdom". In: *Nature Communications* 13.1 (June 2022), p. 3358. ISSN: 2041-1723. DOI: 10.1038/s41467-022-31038-4.

[59] Aidan P. Thompson et al. "LAMMPS - a Flexible Simulation Tool for Particle-Based Materials Modeling at the Atomic, Meso, and Continuum Scales". In: *Computer Physics Communications* 271 (Feb. 2022), p. 108171. ISSN: 0010-4655. DOI: 10.1016/j.cpc.2021.108171.

[60] Maxime Tourte et al. "Functionalized Membrane Domains: An Ancestral Feature of Archaea?" In: *Frontiers in Microbiology* 11 (Mar. 2020), p. 526. ISSN: 1664-302X. DOI: 10.3389/fmicb.2020.00526.

[61] Marleen van Wolferen et al. "The Cell Biology of Archaea". In: *Nature Microbiology* 7.11 (Oct. 2022), pp. 1744–1755. ISSN: 2058-5276. DOI: 10.1038/s41564-022-01215-8. PMID: 36253512.

[62] Victoria Vitkova et al. "Elasticity and Phase Behaviour of Biomimetic Membrane Systems Containing Tetraether Archaeal Lipids". In: *Colloids and Surfaces A: Physicochemical and Engineering Aspects* 601 (Sept. 2020), p. 124974. ISSN: 09277757. DOI: 10.1016/j.colsurfa.2020.124974.

[63] Xin Wang and Markus Deserno. "Determining the Lipid Tilt Modulus by Simulating Membrane Buckles". In: *The Journal of Physical Chemistry B* 120.26 (July 2016), pp. 6061–6073. ISSN: 1520-6106. DOI: 10.1021/acs.jpcb.6b02016.

[64] Rui Xu et al. "Elastic Property of Membranes Self-Assembled from Diblock and Triblock Copolymers". In: *Chemistry and Physics of Lipids* 221 (July 2019), pp. 83–92. ISSN: 00093084. DOI: 10.1016/j.chemphyslip.2019.03.015.